

School of Earth and Planetary Sciences

Sensors Utilisation and Data Collection of Underground Mining

Fatemeh Moghaddam

**This thesis is presented for the Degree of
Master of Philosophy (Surveying and Mapping)
of
Curtin University**

December 2022

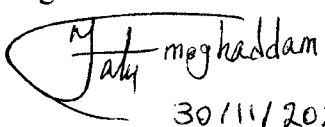
DECLARATION OF AUTHORSHIP

I, Fatemeh Moghaddam, declare that this thesis titled, "Sensors Utilisation and Data Collection of Underground Mining" and the work presented in it are my own. I confirm that:

- This work was done wholly or mainly while in candidature for a research degree at this University.
- Where any part of this thesis has previously been submitted for a degree or any other qualification at this University or any other institution, this has been clearly stated.
- Where I have consulted the published work of others, this is always clearly attributed.
- Where I have quoted from the work of others, the source is always given. With the exception of such quotations, this thesis is entirely my own work.
- I have acknowledged all main sources of help.
- Where the thesis is based on work done by myself jointly with others, I have made clear exactly what was done by others and what I have contributed myself.

Fatemeh Moghaddam

Signature

 Fatemeh Moghaddam
30/11/2022

ABSTRACT

Nowadays, drones are increasingly being used in industrial and environmental applications. In particular, there is significant demands for adapting drones for use in underground mining. Due to the lack of GPS signals in an underground mine, successful usage of a drone in such a rugged space requires accurate and reliable positional information to achieve safe underground navigation. The implementation of two modules help overcome the challenge. Firstly, a module to find global coordinate values of underground locations and track changes in the position and orientations of the drone. Secondly, a module with the ability to generate and map the area for accurate localisation and the collection of 3D images of the underground mine. In both modules, an Inertial Measurement Unit (IMU) plays a major role in collecting data location and sending it to the appropriate processing unit. The IMU is made of three components, including accelerometers, magnetometers, and gyroscopes. Its limitation is that errors accumulate and propagates over time, leading to drift in the position and attitude solutions. Various methods must be applied to mitigate this error enabling precise positioning and mapping.

This study primarily reviews the significance and performance of IMUs for underground mine drone localisation and mine mapping. IMUs are one of the most important devices for navigation. To address attitude drift, this research has designed a Kalman Filter (KF) which extracts reliable information from raw data. The KF for INS combines different measurements while considering estimated errors to produce a trajectory which includes time, position and attitude. To evaluate the feasibility of the proposed novel method, a prototype has been designed and evaluated. Experimental results indicate that the designed KF estimates the internal states of a system (roll, pitch and yaw) in the presence of uncertain and indirect measurements (heading and distance).

The test setup was designed to allow the application of specific algorithms and viewing the results of different scenarios for better understand position and orientation determination using the IMU MPU 9250. The purpose of all tested scenarios was to observe the IMU's performance and ability in the presence of sudden acceleration and

deceleration of the system. All figures illustrate that the KF at the end of the timing period makes the presented curves more stable and smoother, providing a better representation of the true movement occurring in the system. Due to sudden changes in the system, drift increases exponentially, which causes a delay in the KF's performance.

Key terms: Kalman Filter (KF), Inertial Measurement Unit (IMU), Calibration, Indoor Navigation

ACKNOWLEDGEMENTS

First and foremost I am extremely grateful to my supervisors, Dr. David Belton, Dr. Petra Helmholz, Dr. David McMeekin and Prof. Iain Murray for their invaluable advice, continuous support, and patience during my Master study. Their immense knowledge and plentiful experience have encouraged me in all the time of my academic research and daily life. I would also like to thank Dr. Azadeh Nazemi for her technical support on my study, without her technical support and advice this research would not be possible. Finally, I would like to express my gratitude to my husband and my daughter. Without their tremendous understanding and encouragement in the past few years, it would be impossible for me to complete my study.

ATTRIBUTION STATEMENT

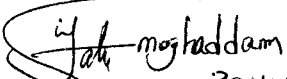
	Conception and Design	Acquisition of Data and Method	Data Conditioning and Manipulation	Analysis and Statistical Method	Interpretation and Discussion
Co-Author 1 (Fateme Moghaddam)	30%	60%	70%	40%	50%
<p>Co-Author 1 Acknowledgment: I acknowledge that these represent my contribution to the above research output and I have approved the final version.</p> <p>Signed:  Fateme Moghaddam 30/11/2022</p>					

TABLE OF CONTENTS

DECLARATION OF AUTHORSHIP	ii
ABSTRACT	iii
ACKNOWLEDGEMENTS	v
ATTRIBUTION STATEMENT	vi
TABLE OF CONTENTS	vii
LIST OF FIGURES	x
LIST OF TABLES	xii
1. INTRODUCTION	1
1.1 Project Background.....	1
1.2 Aim and Objectives.....	6
1.3 Significance.....	7
1.4 Chapter Summary.....	7
2 REVIEW OF LOCALISATION AND POSITIONING METHODS	9
2.1 Introduction	9
2.2 Overview of underground mining operations - Manual, Semi-Autonomous and Autonomous	9
2.3 Unmanned Autonomous Vehicles (UAVs) solutions used in underground mine sites.....	10
2.4 Unmanned Aerial Vehicles (UAVs/Drone) and Sensor Selection.....	13
2.4.1 Data collection using capturing device of the external environment.....	14
2.4.2 Data collection using external sensor for drone information.....	16
2.4.3 Data Collection using Inertial Navigation for drone orientation	19
2.5 Examples of commercial UAVs systems.....	20
2.5.1 Hovermap System	20
2.5.2 Elios System.....	22
2.5.3 M2 System	22
2.5.4 Batonomous System.....	23
2.5.5 Summary of systems	24
2.6 Chapter Summary.....	25
3 REVIEW OF POSITIONING AND LOCALISATION USING IMU.....	26
3.1 Introduction	26

3.2	Inertial Measurement Unit (IMU) components.....	26
3.2.1	Accelerometer	26
3.2.2	Gyroscope	27
3.2.3	Magnetometer	28
3.2.4	Selecting an IMU for UAV Applications.....	28
3.2.5	Using IMU components to measure roll, pitch and yaw.....	30
3.3	IMU for positioning and orientation in UAV system	34
3.4	Errors, initialisation and compensation.....	36
3.4.1	Initialisation and calibration of IMU	37
3.4.2	Compensation and information fusion.....	38
3.5	Filtering	40
3.5.1	Principal of filtering	41
3.5.2	Complementary filtering	42
3.5.3	Kalman Filtering	43
3.6	Chapter Summary.....	45
4	IMU FILTERING METHODOLOGY AND PROTOTYPE	47
4.1	Introduction	47
4.2	Filtering Implementation.....	47
4.3	System Prototype	56
4.4	System Implementation.....	57
4.4.1	System Synchronisation.....	57
4.4.2	Accelerometer, Gyroscope and magnetometer synchronisation.....	58
4.4.3	Synchronisation required for communication between IMU device and processing device.	59
4.4.4	First approach – Using RPi only	60
4.4.5	Second approach – Using Arduino and RPi.....	62
4.5	Chapter Summary.....	63
5	EXPERIMENTAL RESULTS.....	64
5.1	Introduction	64
5.2	IMU specifications	65
5.3	Initialisation and Calibration.....	65
5.4	IMU filtering results overview.....	66
5.4.1	Dropping scenario	67

5.4.2	Double tap Scenario	71
5.4.3	Walking scenario.....	75
5.4.4	Horizontal nudge of IMU.....	78
5.4.5	Fast pickup IMU	81
5.4.6	Slow pickup of IMU	83
5.5	Chapter Summary.....	87
6	CONCLUSIONS.....	88
7	REFERENCES.....	94

LIST OF FIGURES

Figure 1.1 Research Steps	7
Figure 2.1 Markers define the start and end of the desired route.....	12
Figure 2.2 Overview diagram of available sensors for UAVs/Drone systems	14
Figure 2.3 Emesent’s Hovermap Mining payload (Hovermap, 2019).....	21
Figure 2.4: Flyability’s Elios (Flyability, 2014)	22
Figure 2.5 Near Earth Autonomy’s M2 (Autonomy, 2016).....	23
Figure 2.6 Inkonova’s Batonomous (Inkonova, 2018)	24
Figure 3.1 Piezoelectric accelerometer (Woodford, 2020)	27
Figure 3.2 Capacitive accelerometer (Woodford, 2020).....	27
Figure 3.3 Roll (vertical movement), Pitch (horizontal movement) and Yaw for heading (Thuillier, 2018)	31
Figure 3.4 Dead Reckoning method based on integrated accelerometer and the gyroscope to find position and orientation.....	35
Figure 3.5 KF state estimation	43
Figure 4.1 Kalamn Filter (KF) Implementation.....	49
Figure 4.2 Unknown obstacle estimation by IMU and capturing device.....	57
Figure 4.3 First approach prototype	61
Figure 4.4 Second approach prototype.....	63
Figure 5.1 Drone autonomous positioning system overview.....	64
Figure 5.2 The raw measurements for the roll data (red) plotted against the data processed by the KF (blue) for the dropped scenario.	68
Figure 5.3 The raw measurements for the pitch data (red) plotted against the data processed by the KF (blue) for the dropped scenario.	69
Figure 5.4 The raw measurements for the yaw data (red) plotted against the data processed by the KF (blue) for the dropped scenario	70
Figure 5.5 The raw measurements for the roll data (red) plotted against the data processed by the KF (blue) for the double tap scenario.....	72
Figure 5.6 The raw measurements for the pitch data (red) plotted against the data processed by the KF (blue) for the double tap scenario.....	73
Figure 5.7 The raw measurements for the yaw data (red) plotted against the data processed by the KF (blue) for the double tap scenario.....	74

Figure 5.8 The raw measurements for the roll data (red) plotted against the data processed by the KF (blue) for the walking scenario.....	75
Figure 5.9 The raw measurements for the pitch data (red) plotted against the data processed by the KF (blue) for the walking scenario.....	76
Figure 5.10 The raw measurements for the yaw data (red) plotted against the data processed by the KF (blue) for the walking scenario.....	77
Figure 5.11 The raw measurements for the roll data (red) plotted against the data processed by the KF (blue) for the horizontal nudge scenario.....	78
Figure 5.12 The raw measurements for the pitch data (red) plotted against the data processed by the KF (blue) for the horizontal nudge scenario.....	79
Figure 5.13 The raw measurements for the yaw data (red) plotted against the data processed by the KF (blue) for the horizontal nudge scenario.....	80
Figure 5.14 The raw measurements for the roll data (red) plotted against the data processed by the KF (blue) for the fast pickup scenario.....	81
Figure 5.15 The raw measurements for the pitch data (red) plotted against the data processed by the KF (blue) for the fast pickup scenario.....	82
Figure 5.16 The raw measurements for the yaw data (red) plotted against the data processed by the KF (blue) for the fast pickup scenario.....	83
Figure 5.17 The raw measurements for the roll data (red) plotted against the data processed by the KF (blue) for the slow pickup scenario	84
Figure 5.18 The raw measurements for the pitch data (red) plotted against the data processed by the KF (blue) for the slow pickup scenario	85
Figure 5.19 The raw measurements for the yaw data (red) plotted against the data processed by the KF (blue) for the slow pickup scenario	86

LIST OF TABLES

Table 2.1 Summary of the sensors and their ranges	19
Table 3.1 MEMS IMUs Comparison.....	30

1. INTRODUCTION

1.1 Project Background

This research project studies the use of autonomous Unmanned Aerial Vehicles (UAVs) or drones, specifically for the mapping and surveying underground mining applications. Based on the safety regulations in underground mines, localisation and mapping are essential requirements for mine operation. A possible solution is to utilise drones with self-navigation capabilities and to equip them with positional sensors, namely the Inertial Measurement Unit (IMU), to map the required areas. This research focuses on low cost IMUs to propose a cost-effective method for localisation and mapping. The aim of this research is to improve the accuracy of the IMU data provided for drone localisation and consequently for mapping. Specifically, the research looks at improving the raw IMU data through filtering methods to reduce the negative impact of IMU drift over long distances.

The mining industry is currently experiencing rapid change and mineral resources play a significant role for developing countries as a source of income. Australia has invested in mining innovations that benefit from its resource sector, by achieving sustainable levels of output and decreased production overheads (Phillips, 2012). Many of these innovations have been focused on satisfying and improving the stringent health and safety regulations around the Australian mining industry. Health and safety plays a major role in the mining industry in Australia (Heber, 2013). According to these regulations, workers can only be sent into areas of an underground mining operation after ensuring that the environment is safe. This is an increasing concern as underground operations become deeper as more ore is extracted due to increase resource prices and profitability. One way of addressing these safety concerns is through automation, by removing individuals from potentially unsafe environment.

The method of mining employed depends on the type and structure of the resources being mined. For example, in gold mining a typically used method is vertical mining where mining occurs from the bottom of the deposit, and proceeds upwards with the

ore being collapsed in layers downwards (Phillips, 2012). This results in open voids called stopes, which are hazardous environments due to a lack of ground support, inadequate ventilation, little accessibility, and little to no lighting. These are usually accessed by a near-horizontal tunnel running parallel to the strike of the ore body, referred to as drives. The width of a drive is typically constant and drives are “classified” based on their width, such as 4-metre drive, 5.5-metre drive, and 2.5-meter drive. The majority of the drive length is dug out at a minimum height and is usually measured similarly to its width. The backs (or roofs) are curved to increase strength. There are instances where the height of the drive needs to be increased to accommodate loading operations. If the drive is made of non-competent rock, it often needs additional support (such as shotcrete or rock bolts) before it is considered safe to access. Throughout these works, environmental conditions such as air flow, temperature and air quality are critical to ensure safe operations. In addition, heavy traffic and the inability to shut down drives (due to cost in loss of productivity) can make access an issue at times.

Mapping and surveying the extents of these and other mine workings is of critical importance throughout the life cycle of a mine. It is used not only in mining development and resource production but also as part of the regulations. An example of these requirements can be found in the Resources Safety Matters publications for workplace safety and health in Western Australia (Mine, 2021). Resources, utilities, access, and dimensions need to be mapped and surveyed. As mentioned previously, access to underground mine tunnels can be restricted or prohibited in some instances (Anderson, 2013). Due to their potential hazardous or restrictive nature, mapping the correct structure, layout, and resource location without exposing individuals to an unsafe environment, as well as accurate mapping to help reduce cost and increase productivity, is one of the most important reasons why mine are seeking autonomous surveying and mapping technology.

Over the years, many solutions have been proposed in research to reduce or eliminate the need to directly access certain areas of mine sites. To address these limitations, autonomous or semi-autonomous methods are often utilised. One of the most important aspects of achieving this is ensuring that the vehicle or platform used is

aware of its location in relation to the surrounding environment, which makes localisation essential.

Many approaches for achieving accurate positioning and localisation in underground mining tunnels are based on indoor navigation techniques. For example, systems based on indoor wireless positioning methods can be used. These systems rely on distance measurement using wireless signals and are designed for short distance wireless communication (Yuping et al., 2014). However, wireless positioning methods require significant processing time, and the equipment used is not cost-effective. Additionally, due to the surrounding rock absorbing and blocking signals, such methods cannot be deployed for use over long distances in underground mine sites.

As a result, the Australian mining industry has implemented forms of remote control for autonomous and remote operation technologies. Machinery and mining processes are performed and supervised remotely from the mine shaft, with Unmanned Aerial Vehicles (UAVs) being a common solution across sites (He et al., 2019).

Over the last two decades, there has been a significant focus on the development of autonomous vehicle and remote operation technology in underground mining. (J. N. Bakambu et al., 2004) (Cox, 1991) (Alami et al., 1998) (Roberts et al., 2000) (Madhavan et al., 1998). Bakumba et al (2007) specially described two modes of operation for autonomous platform in underground mines: navigation and surveying modes. These operations are used in networks of tunnels in underground mines (Joseph Nsasi Bakambu et al., 2007). An integrated architecture that enables a mobile robot to perform corresponding actions while controlling their execution in real-time and being reactivate to possible events. (Alami et al., 1998). This architecture includes three levels: functional, execution and decision making. The functional level involves effector control and sensor data processing, while the execution level coordinates and controls the execution of distributed functions. The decision level (or final level) produces the task plans and supervises the execution. All levels are necessary for an autonomous robot to perform effectively.

Roberts et al (2000) reviewed the navigation techniques, such as absolute and reactive navigation. The reactive navigation approach is based on wall following and the use of a primary sensor, such as a laser scanner (Roberts et al., 2000). In another study, Madhavan and Durrant used laser scanning sensors to develop a localisation algorithm. They combined an Iterative Closest Point (ICP) algorithm with an Extended Kalman Filter (EKF) to create the ICP–EKF method (Madhavan et al., 1998). The ICP–EKF uses the ICP algorithm to localise an autonomous robotic vehicle in relation to pre-made mapping.

UAVs also perform positioning using systems that determine absolute coordinates, such as indoor wireless positioning, which rely on WIFI (Yuping et al., 2014) or Global Navigation Satellite System (GNSS) which is based on GPS and other satellite systems. Standard UAV navigation system rely on GNSS and inertial sensors (INS).

However, in the absence or weakness of GNSS signals underground, the INS alone would drift over time, and the state estimation provided by INS would be unreliable due to error accumulation. Moreover, rocks in the underground mine can interfere with or block radio communication, making remote piloting impossible.

Therefore, in the rugged space of an underground mine, self-navigation of the drone requires accurate positional information. A fully autonomous, self-localisation solution is required due to the lack of external positioning. The utilisation of drones in the underground setting involves the implementation of self-navigation and finding global coordinate values of underground locations known to the operator, such as in the form of signs or located and exiting features.

In summary, an autonomous system requires accurate localisation along its path by utilising mapped features that can be observed by the drone as it captures local surrounding features during operation. Consequently, this map of features plays an important role in piloting the autonomous system and assisting its self-positioning. The drone can determine its location in the underground environment utilising targets, naturally occurring features, and elements in the scene that have been previously mapped.

Using unique features located on mine walls such as landmarks is a suitable alternative technique for localisation. Scanning laser sensors are a common choice for detecting these natural landmarks. However, laser sensors are unreliable in dusty and other similar conditions due to cost factors, power and computing requirements, and weight limitations. These factors all contribute to the unpredictability of the sensors. More advanced methods such as Simultaneous Localization and Mapping (SLAM) and block modelling are required for this task.

The SLAM method builds a map and localises the vehicle in the map at the same time (Bailey et al., 2006) using features that have previously been mapped and are known to the algorithm. SLAM operates based on two steps:

- Using feature extraction to generate preliminary feature maps and coordinate.
- Using feature matching, state evaluation, as well as state restoration and map management to recognise previously mapped features, which are then used to localise the drone (James et al., 2012).

Another method for localisation in mining operation is the block model, where the ore body is represented as a stack of multiple computer generated bricks. Each brick corresponds to the ore grade, density, volume, and other geological or engineering data. The block model cells are arranged in an XYZ grid system, and can be of uniform or irregular size (Report, 2003). The data generated by block modelling can be used in various mathematical methods for estimating mapping and localisation.

The discussed methods all require additional information on the orientation and attitude of the system, which is usually achieved using Inertial Measurement Units (IMU) either alone or in conjunction with other information. This research is focused on how to use an IMU sensor to obtain position, velocity, and attitude information based on the measurements taken by the IMU for an autonomous system. The IMU contains three sensors that are sensitive to noise and accumulate errors over time, so an appropriate filter must be selected to address the noise issues, such as Kalman (Noureddin, 2013) or Complementary (Higgins, 1975) filtering methods, in order to

reduce their effect. This can be further aided by integrating information from a distance capturing device and applying the Dead Reckoning (DR) principle.

1.2 Aim and Objectives

This research aims to propose a cost-effective method for localisation of drones in underground mine sites using low cost IMUs. While these IMUs are smaller and cheaper, they may generate poor quality data. However, with proper processing, the IMU can supply the required information for the navigation system and plays a critical role in drone positioning methods. It is important to note that data captured by an IMU is unreliable for long distances due to attitude drift, which accumulates exponentially, especially when using low-quality data capturing devices. Therefore, the data received from an IMU needs to be processed to calculate changes in the drone's position and orientation, to improve the quality of the output, and reduce drift and errors introduced by noisy data.

The aim of this research is to improve the accuracy of localisation by enhancing the quality of IMU data. Specifically, the research focuses on mitigating the negative impact of IMU drift in long-distance operations through filtering methods. The proposed model corrects the collected raw data to provide more accurate navigation information, effectively reducing the impact of environmental noise and sensor drift.

To achieve the aim of this research the following steps are preformed:

- IMU device initialisation and calibration based on the device datasheet.
- Implementation and comparison of a filtering method (Kalman Filter-KF) with the use of raw data to test the device at rest, and in motion over a period of time as it will be described in experimental result section.
- Data Collection to obtain reliable information and calculate the orientation and position after the starting point using IMU data.
- Quantifying the reduction in drift and noise of the IMU device base on time and displacement.

The filtered IMU data can then be used for determining the location of the drone. Figure 1.1, illustrates the steps to produce the system's positioning data which combines the outcomes from the IMU filtering data.

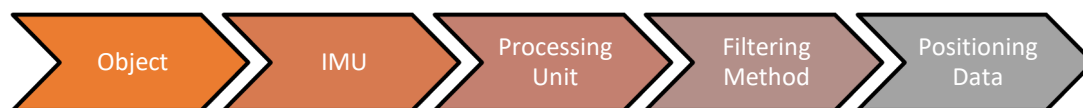


Figure 1.1 Research Steps

1.3 Significance

The significant contribution of this research is to assist in developing a localisation system for hazardous mine environments by accurately positioning drones using low cost and small IMU sensors commonly used due to weight or cost considerations. The high sampling rate of IMU data makes it an ideal candidate to collect position and orientation data. However, the obtained information is only accurate for a short period, and over time, it may gain integration drift. The improved position data will contribute to precise mapping using drones, and combining the filtered IMU data with other sensors or methods such as SLAM can further improve it. This research aims to improve IMU data capturing and increase autonomous navigation.

1.4 Chapter Summary

This chapter introduced the project's background, aims, detailed its objectives, and explained the research significance and the method that will be implemented. In the next chapter, background information will be provided based on reviewing existing literature and systems with respect to localisation using sensors. Chapter 3 will describe the essential concepts related to IMU and its components, the internal states of a system (roll, pitch and yaw), IMU errors, initialisation and compensation, the filtering principal, and explain complementary and Kalman filtering. Chapter 4 will evaluate the IMU significance and performance for the localisation of drones in underground mine sites, followed by the steps for designing the KF method. It will

also detail a prototype design used in this research, including an investigation of its advantages and disadvantages. Experimental and evaluation results are available in chapter 5. Finally, chapter 6 contains the conclusion that low cost IMUs provide a cost-effective method for localisation and mapping and a discussion of further possible developments.

2 REVIEW OF LOCALISATION AND POSITIONING METHODS

2.1 Introduction

The use of Unmanned Aerial Vehicles (UAVs) are increasingly prevalent in industrial and environmental applications. Specifically, there is a growing demand on adapting drones for use in underground mining (Shahmoradi et al., 2020). Due to the need for drones to collect data in inaccessible areas, numerous techniques have been developed to overcome the positioning problem and enable safe indoors or underground navigation (Jinhong et al., 2011). This chapter aims to review existing research and practical approaches for underground mine localisation and evaluate their advantages and limitations. In particular, the chapter focuses on:

- Reviewing existing mining operation systems that use different technologies for localisation and positioning in a mine,
- Briefly describing the methods and their advantages,
- Introducing and implementing low cost IMU for positioning and localisation;
- Explaining how this research contributes to addressing the localisation issue.

2.2 Overview of underground mining operations - Manual, Semi-Autonomous and Autonomous

Mining operations can be broadly classified into three main categories: Manual, Semi-Autonomous and Autonomous. In Manual operations, all tasks are completed entirely by human operators. Although the system may have certain automated features such as collision avoidance the operator remains in control throughout the entire task. Equipment can either be manned or remotely controlled. For example, manually filling the bucket of a vehicle manually at a draw point under operator control is an example of the first category.

In Semi-Autonomous operation, the system performs certain tasks autonomously within a set of defined operations and without direct human intervention or control. For instance, a semi-autonomous vehicle can be utilised to survey a mine shaft and

collect data. Initially an operator drives the vehicle between datum points to teach the system the required route. Then, the system can guide the vehicle on its route between two “markers” that define the start and end of the desired route, using the route it learned during the first time manual guidance.

Finally, in Autonomous mode, the system is capable of sustained autonomous operations and has situational awareness without any operator input. For instance, a pre-recorded map can be loaded into the vehicle system, and the vehicle can navigate independently by scanning its surrounding area and comparing the captured data to the provided map to localise itself. Pathfinding algorithms can then be used to automatically determine the best path to the destination (Larsson et al.).

2.3 Unmanned Autonomous Vehicles (UAVs) solutions used in underground mine sites

The tasks that UAVs perform in mine operation include resource location, stability analyses, safety inspections, as well as dimension and stope mapping (Anderson, 2013). For example, UAVs are capable of passing through locations and spaces that are difficult to access by people or equipment, making them ideal for exploring shaft entrances and passes where access is limited. Stope mapping is an example of UAV applications in underground mining (White et al., 1975). Stopes are inaccessible for human entry due to instability and a lack of roof protection and support. As previously mentioned, these cavities suffer from specific underground conditions such as being unsafe, not properly ventilated, with little accessibility, lighting, and no support and reinforcement of the ground, walls, and roofs. The advantages of using UAVs are that it allows for direct access to the stope without endangering human operators.

UAVs used in the underground mine environments commonly face issues related to time efficiency and cost. The operation of UAVs is time-consuming and requires specialised platform and sensors, resulting in high cost associated with underground drone mapping. In contrast, other methods such as cavity monitoring systems are quick to setup and capture data. However, UAVs overcome specific challenges in the

mining environment problems such as dust, humidity, darkness, and air ventilation, which can be a difficult for human operators to navigate. UAVs also have the advantage of accessing spaces that may not be accessible to human operators, resulting in more complete coverage of data capture. However, UAVs, still require some level of manipulation in unpredictable mining environments to improve their performance. UAVs belong to the Autonomous category of mining operations, but in certain situations, they require manual intervention.

In the mining industry autonomous and remote operation technologies have evolved using various forms of remote control. Firstly, machinery and mining processes can be performed and supervised remotely from the secure mineshaft. Remote operations can include drilling which is performed by workers using a remote control from a distance, and direct tele-operations, such as controlling the mining process from a computer in a control room (McNab, 2012). Secondly, semi-autonomous vehicles can also be used for such applications. However, semi-autonomous vehicles still lack sufficient accuracy, can be complicated to operate, and often require long and monotonous working hours. Although some assigned tasks still require human interaction, resulting in the issues mentioned above. A semi-autonomous vehicle does not pose significant challenges. Switching to an autonomous system would require retrofitting existing equipment, which is costly and involve a redesign of on-board systems (arcelormitta, 2021).

Semi-Autonomous operation are currently being used is vertical gold mining to map the area where the ore has been, or will be extracted. One technique used in Western Australian gold mines is the use of an Unmanned Semi-Autonomous Vehicle (USAV) (Larsson et al., 2006). The USAV is driven between datum points by an operator to teach it the required route to be captured. This route includes flying from the drive, through the access into the stope, and then back out again. Once the drone has learnt this route, it can repeat it autonomously. However, there are some restrictions and potential problems with using USAVs. Inaccuracy in the measurements of the drone's position is a significant issue, as is the time intensive process required to provide the required initial map to which the drone will operate. Safety concerns arise for the

operator creating the map, such as poor ventilation, limited accessibility and, lack of support and reinforcement of the ground and roofs.

To survey the stope, surveyors scan it using a tripod based laser scanner on the end of a boom extended into the space. However, a complete model cannot be captured due to the shape of stopes occluding portions of it. This means that only approximate measurements can be derived, raising the risk of high inaccuracies in the results. To ensure the USAV operates smoothly inside a drive, it requires the use of the “point-to-point” mode where the vehicle will drive itself until it reaches its destination identified by a marker. The drive dimension or the opening of the mine it is travelling through need to be known to use this mode. Fixed survey markers such as a white painted triangle on the wall with a bolt drilled in the middle provides a fixed datum point in 3D space. Alternatively other markers can be used as long as they are distinct and recognised by the system, such as the one depicted in Figure 2.1.



Figure 2.1 Markers define the start and end of the desired route

Bakamba et al., developed a system with similar navigation capabilities as mentioned above (Joseph Nsasi Bakambu et al., 2007). They proposed a system with two modes of operation: surveying and navigation mode. In the surveying mode two- and three-dimensional maps are produced by utilising artificial landmarks for drone localisation and range measurement obtained by two orthogonal scanning laser sensors for the mapping. In navigation mode, maps produced during surveying mode are used to conduct high-level missions, including automated detection of natural landmarks for self-localisation and pre-planned navigation moves. The autonomous vehicle uses

sudden changes in the corridors, bays and intersections of the local structure to identify and localise natural landmarks. Bakambu uses point-to-line segment matching instead of point-to-point matching similar to that described by Cox (1991). (Cox, 1991), (Makela, 2001) Another method for localisation in underground mines using laser scanning sensors is described by Makela. In this method, Makela describes Load Haul Dump (LHD) using the wall's profile to correct for Dead Reckoning drift by vehicles autonomously navigating through a mine. To measure the wall's profile, this algorithm uses laser scanning. It's compared to a pre-made model of the environment built from range data compiled while an operator manually drives a route. At every location it is assumed that the wall profile is uniquely identifiable, its measurements can be used to determine the vehicle location and correct it within a reasonable uncertainty using a filtering method.

In a nutshell, the main disadvantage of the USAV approaches is the requirement to provide the algorithms with precise pre-made maps and the lack of such surveying information and existing data in mine sites. In summary, in the next subsection Unmanned Aerial Vehicles (UAVs/Drone) will be reviewed as well as the sensors required, based on the aims of this research for localisation and simultaneous surveying/mapping.

2.4 Unmanned Aerial Vehicles (UAVs/Drone) and Sensor Selection

Unmanned Aerial Vehicles (UAVs/Drone) are increasingly used in industrial and environmental applications, there are significant demands on adapting drones in underground mining. The increase use of drones in inaccessible areas to collect data has led to development of many techniques to overcome the positioning problem and to be able to safely navigate indoors or underground. Sensors play a major role in localisation and positioning in UAVs (Shahmoradi et al., 2020).

Figure 2.2, illustrates the drone mine localisation and positioning systems based on sensor availability. To navigate a drone in an underground mine, three different types of sensor are used. The first type of sensor captures the external environment using different technologies, such as LiDAR (Light Detection and Ranging), SONAR and

cameras. The second type of sensor, inertial sensors such as IMUs, are used to recognise the drone's movement. Finally, external sensor such as GNSS, wireless, and captured targets are used to provide the drone with information for localisation and positioning.

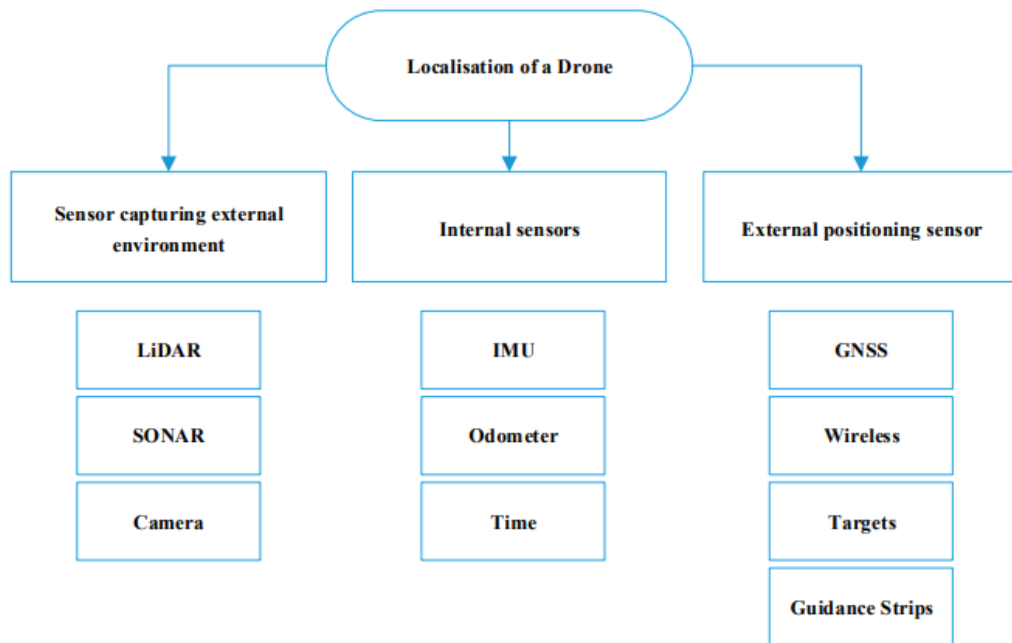


Figure 2.2 Overview diagram of available sensors for UAVs/Drone systems

Various data such as location and distance derived from these sensors can be used for collision avoidance, positioning, mapping, and decision making. As the research is based on the assumption of using drones as an autonomous system, only data collection using sensors enabling an autonomous system is reviewed in the following sections. The information provided by these sensors also enables the capability of minimising collisions or loss of UAVs/Drone.

2.4.1 Data collection using capturing device of the external environment

There are different sensors which capture information about the external environment, such as LiDAR, SONAR and camera. LiDAR is a technology that uses a laser to measure distances (Bottasso et al., 2014). The data captured by LiDAR include

measurements from a single beam or from multiple lines. LiDAR systems use ultraviolet, visible, or near-infrared light as the main medium to measure distances. Furthermore, LiDAR systems can be categorised as pulse or phase system, depending on the method used to measure the distance to an object. Pulse systems refers to the light impulse emitted by LiDAR systems, which is measured on its return after being reflected from the object. The time which the pulse takes to return to the sensor is measured, and the distance to the objects is calculated as the speed of light is known. (Donovan et al., 2009). A Phase system uses the modulation in the amplitude or frequency in the carrier wave. The phase difference between the emitted and detected signal is calculated to determine the time of flight and distance.

Initially, LiDAR systems only worked with single returns of the first and last pulse return, but recent systems can often provide at least three returns per pulse. It is also possible to digitise the full wave form of the pulse returning to the scanner. Common methods are to measure multiple returns, which capture between three to five returns per pulse. There will be an increase in the amount of data as well as the ability to determine the three-dimensional structure of the surface (Vázquez-Arellano et al., 2016). The data from LiDAR can be presented in different formats such as points (in form of point clouds), as well as lines, and surfaces derived from the point measures. LiDAR systems have advantages and disadvantages when it comes to autonomous UAV systems. Some system designs help to bridge gaps concerning feature depth sensing, angular resolution, and low complexity processing (Kapusta, 2020). However, erroneous pulses are easy to create within this system. This in turn influences the detection of already existing objects as either further or closer than they truly are (cprime, 2020). LiDAR sensors help UAVs detect the surrounding environment and the exact distance to an object's position. This requires power consumption as they detect objects by transmitting lasers. However, LiDAR sensors continuously consume power inefficiently which has an effect on autonomous system using and requiring significant battery power (S. Lee et al., 2020).

Simultaneous localisation and mapping (SLAM) with LiDAR is a common technique used in semi-autonomous UAVs. SLAM was developed for autonomous systems to locate itself in an unknown environment by simultaneously creating a map of its

surroundings while locating itself within the map (Durrant-Whyte & Bailey, 2006). Due to advantages such as reliability of accuracy, comparatively fast processing time and point density, LiDAR scanners are the best choice of tool for SLAM, whereas Sound Navigation Ranging (SONAR) being lighter in weight and having sufficient mapping accuracy is also considered (Azhari et al., 2017).

SONAR uses sound instead of light and measures the time of the echo in return. When a drone emits a sound pulse, a portion of those waves bounce back off objects in its vicinity, and are recaptured by the SONAR device on the drone. These waves are used to locate distant objects. Obviously, SONAR is more capable of detecting larger items at longer distances better than smaller objects, which implies that the maximum detection distance of the SONAR is dependent on surface area of reflecting object. An advantage of SONAR is its ability to function in rain, snow and, dusty weather. Some newer models are benefiting from higher resolutions and better object recognition capabilities, yet they lack satisfying resolution to detect multiple fast moving or smaller objects. Compared to LiDAR, it has a shorter field of view and accuracy, but is not as expensive or requiring the same level of power usage (Jahromi, 2019).

Cameras are another sensor used by UAVs, allowing for the collection of imagery data. The generated three dimensional digital photogrammetric models from the UAV are used in unsupported excavation and inaccessible areas where other methods requiring human access are not possible. Aguilar et al. (2017) designed a system to develop a method of positioning drones and the orientation with respect to the camera. Their system can run the computation and sensing required for SLAM, removing the dependence on unreliable wireless communication. They make use of visual odometry, loop closure and graph optimisation (Aguilar et al., 2017).

2.4.2 Data collection using external sensor for drone information

Unlike flying a UAV above ground, manoeuvring it underground comes with various difficulties and challenges due to unavailability of communication infrastructures and positioning signals like GNSS. Nevertheless, this following section will describe external sensors to determine the position of a drone using GNSS or Wireless methods.

In above ground autonomous operations, GNSS (which includes the American Global Position System GPS) is usually adopted to calculate absolute coordinates, however due to signal blockage it is impossible to use it in underground mining and other confined spaces. GNSS receiver require a minimum of four visible satellites to determine the location of the receiver using 3-D trilateration. While in theory only three observations are required for 3-D trilateration the fourth satellite is used to solve for the clock error of the satellites (Noureldin, 2013). Other systematic influences and errors of GNSS signals are jamming, spoofing, multipath, or blockage (Tak Kit et al., 2013).

Replacing satellite based systems with wireless systems with known reference locations makes it possible to develop underground wireless positioning. Systems based on this method to position itself and have been adapted for underground mine operations. However, it is very costly (McNab, 2012). When used for the positioning of semi-autonomous vehicles underground, GNSS and wireless systems may result in imprecise measurements for the required task. The positioning accuracy can only be improved through intensive processing, which is time and cost intensive. None satellite based methods use wireless infrastructure (Mostafa et al., 2018).

Furthermore, there are many indoor positioning techniques, utilising methods such as Infrared Data Association (IrDA), ZigBee, Bluetooth, Radio Frequency Identification (RFID), ultra-wideband (UWB) and optical tracking (Jinhong et al., 2011). Le et al. (2018) in their paper provided an overview of the sensor for indoor navigation application. In order to define the absolute position of a movable transmitter using Received Signal Strength Indication (RSSI) evaluation, or Time of Flight (ToF) triangulation; Radio Frequency (RF) sensors such as Wireless connection, UWB, Bluetooth and RFID are utilised. Two primary technologies i.e. Bluetooth and UWB are taken into practice each benefiting from distinct accuracy performance and range. Due to its typical one nanosecond short time pulse duration and maximum 300-meter range, UWB provides accuracies within a centimetre whereas, Bluetooth is less accurate with a greater working range of up to 100 meters. Multi-path reflection and interference with other devices are disadvantages of this sensor family which could

lead to positional glitches by sending wrong positional data to device's auto pilot. (Li et al., 2018).

James, et al. (2012) described a method for localisation and navigation in GNSS denied underground environment, using RFID tags. Different areas are separated and tagged using RFID tags. The system can then detect the area it is localised in through the RFID device detecting the different tags denoting different locations (James et al., 2012). These tags are unable to localise their exact position, however they can find their locality. Subdividing of the studied area by tags is one of the limitations of using RFID in unknown and non-safe environment. Furthermore, this partitioning can only be used for a limited area.

IrDA is another communication system which is based on infrared light point to point communication (Yuping et al., 2014). Infrared light in digital format is adopted to generate 0-1 logic. Note that should there be any obstruction within the communicating devices there will be no data transfer possible. It's limited to be used between two devices and cannot constitute a flexible network. The range of IrDA is one meter and in some situation it can be up to two meters. Networks are created with bypassing devices in which the IrDA takes on the role to share the position information (Yuping et al., 2014).

Bluetooth is a low cost and low consumption power wireless communication method which uses frequency-hopping spread spectrum technology. It operates within short range radio frequency enabling devices such as mobiles and headsets to connect wirelessly (Yuping et al., 2014). Bluetooth devices can establish various networks and easily share their location to find the position of the device. As with IrDA, Bluetooth networks are created with bypassing devices in which the Bluetooth takes on the role to share the position information. Bluetooth can be used to transmit the RF signal which can give the distance from the transmitter to the receiver. (Rongyan et al., 2017)

UWB technology is a communication technology based on sending and receiving extremely narrow nanosecond pulses to transmit data, which has the same magnitude as of the bandwidth (Yuping et al., 2014). UWB can be used for precise indoor

positioning, because travel time of radio waves is dependent on bandwidth, the broader frequency signal has a more accurate signal travel time from transmitter to receiver is measured. The advantages of this system is low power consuming and low complexity and high accurate positioning and it has already be demonstrated to work in an indoor environment (Marcellino, 2018).

ZigBee technology is a short distance technology and designed based on low-power standard LAN protocol (Moridi et al., 2014). ZigBee requires very little energy to forward the data by radio waves from one sensor to another. ZigBee can provide RSSI in underground mines. ZigBee technology is used to construct a wireless sensor network, which will be core for positioning and communications in the system (Xuhui et al., 2010). However, based on working with the frequency is 2.4GHz, it is very vulnerable to signal blockage (penetrating rock for example) and it is not appropriate for underground localisation positioning system.

Sensor Name	Range	Speed of communication
IrDA	1 meter	2400 bits/s to 115,200 bit/s
RFID	Up to 20 meters	13.56 MHz
Bluetooth	10 meters	2.4 GHz
UWB	10 centimetre	3.1 to 10.6 GHz
ZigBee	10-100 meters	250 kbps

Table 2.1 Summary of the sensors and their ranges

Table 2.1 shows the summary of the discussed positioning sensors. All stated methods and technologies used for positioning and designing a localisation system for indoor navigation, however one of the main drawbacks of these sensors are multi-path reflection and interference with other indoor devices.

2.4.3 Data Collection using Inertial Navigation for drone orientation

When collecting data using a UAV, additional flight parameters must be documented that can help to adjust the movement of the drone to ensure a high level of positional

accuracy of the drone. For instance, Inertial Navigation Sensors (INS) help to measure drone location, elevation and orientation. An Inertial Measurement Unit (IMU) is a main component of the INS used in UAVs. The IMU is an electronic device that measures and reports orientation, velocity, and gravitational forces through the use of accelerometers, gyroscopes and often magnetometers. The data collected by an IMU is processed by computers to track position through Dead Reckoning. It is ideal for tracking the state of a drone over a short period of time and for measuring changes in the altitude or orientation, but suffer from integration drift over longer time scales. Hence, IMU data for precise positioning will become unusable after just a few seconds. To overcome this issue, inertial sensors are typically combined with additional sensors and models.

Therefore, a standard UAV navigation system often relies on GNSS as well as the inertial sensors, where the GNSS provides only the position of the drone, but not its orientation. If the GNSS signal becomes unavailable, the state estimation solution provided by the INS can estimate the position of the drone. Furthermore, INS can also use sensors such as pressure for calculating altitude or an odometer to record displacement.

2.5 Examples of commercial UAVs systems

To address the stated challenge of positioning with control and navigating UAVs, several companies are developing UAVs to enhance obstacle detection and avoidance capabilities of the platforms to minimise the potential for a collision. The utilisation of these methods in a GNSS denied environment within drone-based systems is described below. These systems examined are namely the Elios, M2, Batonomous and Hovermap systems.

2.5.1 Hovermap System

One implemented solution is provided by the CSIRO (Commonwealth Scientific and Industrial Research Organisation). The Hovermap system was developed by Ernest

in collaboration with CSIRO in 2019 (Hovermap, 2019). It allows for UAV flights within GPS-denied environments by using a LiDAR based SLAM for obstacle sensing and collision avoidance. Hovermap is based on a light weight variant of the Geo-SLAM ZEB-REVO mobile mapping system designed to be mounted on UAV's (DATA61, 2020). This is provided as the Hovermap payload, and is mounted on a UAV as a complete unit. The payload consists of an on-board, rotating Velodyne Puck Lite (VLP-16) LiDAR scanner included within the Hovermap system. Because of the LiDAR, it is able to identify when the UAV reaches obstacles without the need for further lighting or cameras. A measurement of approximately 300,000 points per second within a range of 100 meter and an accuracy of +/- 30.4 millimetre are accomplished by the VLP-16 (Velodyne LiDAR, 2019). To achieve precise 3D mapping GNSS denied environments, Hovermap employs SLAM algorithms rather than GNSS/INS hardware. LiDAR data is used to generate accurate 3D point clouds which lead to production of precise complex 3D imaging of underground mines. This also means that the system can be used to map indoor and underground opening up many different potential applications. Since LiDAR is used to capture the local environment to map obstacles, it is possible to use this information to determine the location of the vehicle relative to the scene.



Figure 2.3 Emesent's Hovermap Mining payload (Hovermap, 2019)

At the moment Hovermap is one of the only fully autonomous system suitable for underground mine mapping. Although there are other systems provided by other companies, most are only semi-autonomous (such as Elios, M2 and Ernest).

2.5.2 Elios System

Elios is a system that builds solutions for the inspection and exploration of indoor, inaccessible, and confined spaces (Flyability, 2014). It has the ability to fly in environments which are unsuitable for GNSS enabled drones, as well as in dark, troubled air flows and confined spaces. Cameras located on the front of the Elios display a live video feed to the pilot during flight, recording video for later use on an on-board SD memory card. No LiDAR system is integrated for obstacle avoidance, therefore Elios' has a physical barrier between the moving parts of the UAV, and it allows for the detection of obstacles for the user through the interaction of the barrier with the surrounding environment. Elios generates data through the cameras located on the front of the Elios, transmits a live video feed to the pilot during flight and records video for later use on an on-board SD memory card.



Figure 2.4: Flyability's Elios (Flyability, 2014)

2.5.3 M2 System

Near Earth technology (Autonomy, 2016) created a system which is semi-autonomous for indoor mapping. The M2 has propeller guards and consists of a stationary Velodyne Puck Lite (VLP-16) LiDAR scanner which is assembled on a DJI Matrice 100. The M2 system is both limited in autonomy and is pilot controlled. In piloted mode, the UAV is flown independent from collision prevention and object detection sensors. This mode is useful for starting and finishing flights. The autonomous mode is used after take-off and when the UAV reaches an acceptable stabilisation. In autonomous mode, the UAV explores an environment freely without a previously collected map. This UAV is able to complete its mapping by flying over unmapped areas i.e. "map holes" of previously covered areas. It can also be used by hand without the drone to

capture data manually. This means that the mapping can be done autonomously whereas landing needs to be manually performed.



Figure 2.5 Near Earth Autonomy's M2 (Autonomy, 2016)

2.5.4 Batonomous System

Another system is Batonomous, developed by InkonoVA in 2018 for semi-autonomous navigation systems for aerial drones to operate in unknown zones without any infrastructure (Inkonova, 2018). In January 2018, the company INKONOVA released a method called "Laser-based collision avoidance for underground mines." These drones were equipped for laser scanning, LiDAR and Batonomous™.

Batonomous drone has sensors mounted on five sides of the UAV, which are ToF sensors, in addition it also has a front camera. Batonomous systems are also capable of being manually flown by a pilot in both obstacle detection mode on or off. The semi-autonomous mode uses Waypoint Navigation. A Waypoint is a reference point used to define location and navigation, this can be any coordinates (Bianco et al., 2017). In this method LiDAR scanner on the UAV measures distances based on point cloud. In order to initiate a flight, the pilot manually flies the UAV until a connection is established between the UAV and his laptop, this is when the point-cloud is created. Once this connection is verified the pilot will switch to semi-autonomous mode and will only control UAV's horizontal position visually by using the front camera.



Figure 2.6 Inkonova's Batonomous (Inkonova, 2018)

2.5.5 Summary of systems

The four drone systems mentioned for the use within underground mine localisation use similar techniques and sensors, but also differ in some ways. All of the drones above are useable in GNSS denied environments. However, Elios, M2, and Batonomous are all semi-autonomous due to manual take-off and landing. Also Batonomous is restricted by the need of communication with an external computing device (specifically a laptop for data processing). Also it requires the ability to receive control commands from an external system (generally the case) and a pilot as input, while the Hovermap system is fully autonomous.

Although this is the system most desired, the fully autonomous function can be expensive. The SLAM navigational tool combined with inertial measurement unit (IMU) data to improve the accuracy of the position measurements of the UAV and scanner during flight (Paredes et al., 2017).

All the systems utilise IMU in some form. IMU helps to correct changes in the position of the laser from when the pulse is emitted and then received. As such, the research to try and improve this is important in the development of these systems. This research has been conducted to find a low-cost alternative approach for localisation and positioning within underground mines, as well as working amongst GNSS denied environments.

2.6 Chapter Summary

This chapter reviews the current system for localisation and mapping, the drawbacks, and the comparison between manual, semi-autonomous, and autonomous systems as most common methods. It addresses the issues regarding current systems for mapping and localisation in underground mines. Certain components can be replaced or substituted in the system, but most focus on the use IMU and its ability to position or track change over time. Since this study focused on localisation and in particular IMU, the key component is being able to position or track change in position over time which will be exposed in the next chapter. Next chapter contains expanded descriptions about IMUs.

3 REVIEW OF POSITIONING AND LOCALISATION USING IMU

3.1 Introduction

This chapter provides an overview of the Inertial Measurement Unit (IMU) and discusses some of the problems and current solutions in utilising and processing the data from such devices. The chapter first examines what an IMU is and the different components that the system is composed of. Detail is then given on each component, focusing on what they measure and how. A comparison of the different methods and IMU types is given based on price and performance. Finally the methods for examining errors in IMUs are highlighted, including compensation methods and current solutions used to mitigate their effect.

3.2 Inertial Measurement Unit (IMU) components

An IMU consists of a combination of sensors, which allows it to measure and report an object's specific linear acceleration, angular rotation, and magnetic field surrounding the object, using a combination of accelerometers, gyroscopes, and magnetometers. This data can be used to provide position data. An IMU can be attached to a drone and is an ideal device for measuring changes in the altitude or orientation, and to track the state of a drone over a short period of time. Each sensor in an IMU is used to capture different data.

3.2.1 Accelerometer

As the name implies, an accelerometer measures the rate of change in velocity. From a structural point of view they are mainly categorised into two designs: 1) piezoelectric and 2) capacitive. Piezoelectric accelerometers function are based on piezoelectric effect in which a material, e.g. a crystal, generates some electrical charge once subjected to an external force. As Figure 3.1 shows when the accelerometer shifts a mass is moved and exerts a force to a piezoelectric crystal, which generates voltage.

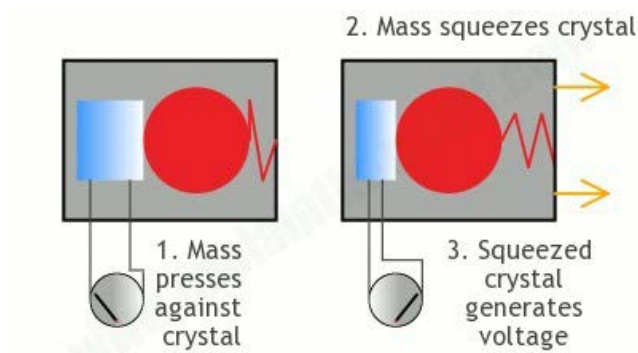


Figure 3.1 Piezoelectric accelerometer (Woodford, 2020)

In a capacitive accelerometer a mass is attached to a variable capacitor in which movement of the accelerometer will cause the capacitor plates to move towards or away from each other, changing the capacitance, hence generating an electric voltage. Figure 3.2 shows capacitive accelerometer functionality in more details.

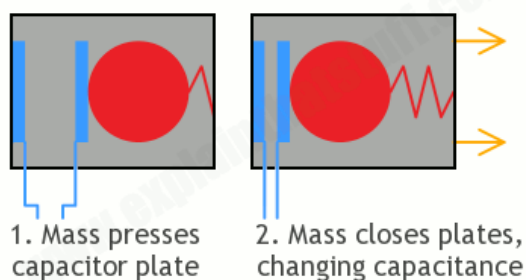


Figure 3.2 Capacitive accelerometer (Woodford, 2020)

Nevertheless, these two methods of measuring acceleration are not practical for light weight devices. Thus Micro Electro Mechanical Systems (MEMS) accelerometers are ideal for use on drones. MEMS Accelerometers are developed based on micro electric manufacturing methods where a microscopic sized sensor is utilised on a silicon chip (Fernandez, 2013) (Shawn, 2020) (Murphy, 2020).

3.2.2 Gyroscope

Gyroscopes are able to sense changes of angular velocity ($\Delta\Omega$) and are conventionally used to maintain the orientation of a device which is moving autonomously. A mechanical gyroscope typically consists of a rotor which is secured in tri-ring gimbals.

The gyroscope working principal is based on a physical phenomenon known as precession (Passaro et al., 2017).

An optical gyroscope such as Fiber Optic Gyroscopes (FOGs) and Ring Laser Gyroscope (RLG) function based on the Sagnac Effect (Barua et al., 2018). Based on Einstein's theory of relativity, if a beam of light in a rotating frame is split into two beams and each beam travels in opposite directions and then are reflected back to the source, they will be out of phase. The relative phase change of the two beams of light will lead to measurement of angular rotation of the ring (Robertson, 1949). MEMS gyroscopes measure the angular rate using the Coriolis Effect. The Coriolis Effect acting on a seismic mass can be detected between the mass and a datum frame of reference, which is rotating in an inertial frame of reference (Kraft et al., 2013) (M. Wang et al., 2018).

3.2.3 Magnetometer

A magnetometer is an instrument for measuring direction and strength of any given magnetic field. In this research magnetometer is used to determine earth's magnetic field which is called the magnetosphere. Strength and direction of magnetosphere is continually changing and its strength depends on location on earth therefore an accurate determination of its strength is paramount. A magnetometer measures any magnetic field in Gauss (unit of magnetic flux) or μT (unit of magnetic field strength). The magnetometer, also known as a magnetic sensor, is a sensor for measuring magnetic induction (magnetic field intensity), which is an important sensor component in all types of aircraft and spacecraft (You, 2018). MEMS Magnetometer measures the earth magnetic field by using Hall Effect or Magneto Resistive Effect (You, 2018). In this method, magnetic sensors convert magnetic or magnetically encoded information into electrical signals for processing by electronic circuits.

3.2.4 Selecting an IMU for UAV Applications

IMUs are essential components in UAV systems due to their application within stabilisation, guidance, correction, as well as measurement and mapping (Dong, 2013).

There are many types of IMU, but the four main technological categories for UAV applications are: Silicon MEMS, Quartz MEMS, Fiber Optic Gyroscopes (FOG), and Ring Laser Gyroscopes (RLG). Among commercially available IMUs the RLG has the highest accuracy, yet this accuracy comes with financial burden. FOG is a cheaper alternative to RLG. FOGs benefit from a design using non-moving parts, which gives them extraordinary rotational precision. Although FOGs are cheaper than RLGs they are still categorised as expensive devices, and other disadvantages of FOGs are the high power consumption and sensitivity to vibrations. Another available option are Silicon MEMS and Quartz MEMS IMUs. MEMS based IMUs offer acceptable performance while benefiting from low power consumption and price tag. Also MEMS are miniature in size and durable when compared to FOGs and RLGs. These characteristics makes them a preferred option for navigation system in drone applications (Passaro et al., 2017).

MEMS IMUs typically perform with higher noise, vibration sensitivity and instability parameters than FOG and RLG IMUs, but MEMS-based IMUs are becoming more precise as the technology continues to be developed (Rees, 2020). MEMS IMUs are ideal for smaller UAV platforms and high-volume production units, as they can generally be manufactured with much smaller size and weight, and at lower cost (Rees, 2020). Although IMUs are popular devices for navigation purposes, they accompany certain amount of error known as drift. Sources of drifts may be due to device physical properties or accumulated rounding values. This drift will lead to significant errors, especially over a long operational period of time. Accuracy of an IMU greatly depends on the quality of its gyroscope. A review of various IMU was carried out by Ahmed et al. They reviewed several IMUs according to various application in different situations (Ahmad et al., 2013).

The Adafruit 9-DOF, PhidgetSpatial Precision, MPU6050 and MPU9250 IMUs are compared in table 3.1 in terms of price, range, interface digital output, degree of freedom (DoF) and frequency. This shows the relative cost and capabilities of such systems.

Title	Adafruit 9-DoF IMU	PhidgetSpatial Precision	MPU 6050	MPU 9250
Price	\$35	\$140	\$12	\$15
Range	± 125 to ± 2000 ($^{\circ}/\text{sec}$)	± 400 or ± 2000 ($^{\circ}/\text{sec}$)	± 250 to ± 2000 ($^{\circ}/\text{sec}$)	± 250 to ± 2000 ($^{\circ}/\text{sec}$)
Interface Digital Output	I ² C, UART	USB	I ² C or SPI	I ² C or SPI
DOF	9	9	6	9
Frequency	12.3 mA (@100Hz)	55 mA (@ 250Hz)	2.96kHz	0.01 dps/ $\sqrt{\text{Hz}}$

Table 3.1 MEMS IMUs Comparison

3.2.5 Using IMU components to measure roll, pitch and yaw

Before explaining how IMU components are used to measure roll, pitch and yaw, a brief explanation on the angular values with respect to the coordinate system (either the global, local, or UAV platform) is provided. In order to study kinematics of a rigid body, two systems of coordinates are introduced, the global coordinate system and the local coordinate system (Ron Harrison, 2007). The global coordinate system is a fix coordinate system to which absolute position to the earth and the motion of an object can be calculated. This is formed as a three dimensional Cartesian coordinate system. In contrast, a local system of coordinates is located in reference to a moving body according to which relative position or speed of the moving rigid body to its instantaneous location or speed is calculated (Thompson et al., 2017). Again, three dimensional Cartesian coordinates can also be used to define a local system of coordinates. A typical example of using Cartesian coordinates is found in the roll, pitch, and yaw of a UAV platform (Park et al., 2016).

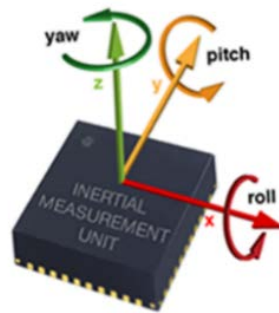


Figure 3.3 Roll (vertical movement), Pitch (horizontal movement) and Yaw for heading (Thuillier, 2018)

An IMU can comprise of a combination of the following: a 3-axis accelerometer that measures acceleration along the X, Y, Z axes define as (a_x, a_y, a_z) , a 3-axis gyroscope that measures angular velocity about the X, Y, Z axes define as (g_x, g_y, g_z) and a 3-axis magnetometer that measures the magnetic field intensity along the X, Y, Z axes define as (m_x, m_y, m_z) of the IMU.

The number of directions for each independent motion measured with respect to each sensor defines the Degrees of Freedom (DoF) for the IMU. There are multiple combinations of DoF such as 6 DoF (3 axis accelerometer, 3 axis gyroscope), and 9 DoF (3 axis accelerometer, 3 axis gyroscope and 3 axis magnetometer) being common configurations. Additionally, 10 DoF can be used in altitude sensor via the addition of a pressure and temperature sensor (Townsend, 2020).

DoF refers to the possible movements of a rigid body within three-dimensional (3D) space. There are only 6-DoF in 3D space, with 3-DoF for linear translation (forward/back, up/down, left/right) and 3-DoF for rotations (pitch, yaw, and roll) (Reliant Systems, 2019). Regardless of the complexity of the movement of a rigid body, its motion can be shown as a combination of these 6 basic DoF. The minimum required DoF is related to each individual application, thus in position tracking it is possible to use 6-DoF in the case of having two sensors or to use 9-DoF in the case of having three sensors (Overholser et al., 2014).

Higher DoF generally means larger sample sizes from various sources, so it can provide more accurate data. Lack of any DoF eliminates relevant data to any given axis, consequently it may generate inaccuracies in the determination of the position of the rigid body. The angular speeds, linear acceleration and magnetic field data measured by an IMU is used to calculate roll, pitch and yaw in order to have position, orientation and velocity of a UAV, by feeding them into a device such as Inertial Navigation Systems (INS).

As seen in Figure 3.3 roll, pitch, and yaw are the movements around the x-axis, y-axis, and z-axis respectively. From this information, position, velocity, and attitude can be measured. The gyroscope provides the angular velocity in three directions and cannot be used to calculate roll, pitch or yaw on its own. The angle can be obtained from the integral of the angular velocity over time and provide access to roll, pitch and yaw tolerances. There are different methods to calculate roll, pitch and yaw each having relevant accuracies which are discussed in following.

Roll is the rotation about the x axis (between -180 and 180 degrees), pitch is the rotations about the y axis (between -90 and 90 degrees) and yaw is the rotation about the z axis (between -180 and 180 degrees). Forces applied to the X, Y and Z axes are captured by the accelerometer as acceleration (ms^{-2}) along those axes. If an object is stationary, only the gravitational acceleration of the earth will be exerted on it. The following equations provide values for pitch and roll, and are valid if the system is not under acceleration, otherwise the values will be affected over the period of acceleration from the movement:

$$\text{pitch} = \text{atan} \left(\frac{a_x}{\sqrt{a_y^2 + a_z^2}} \right) \quad (3.1)$$

$$\text{roll} = \text{atan} \left(\frac{a_y}{\sqrt{a_x^2 + a_z^2}} \right) \quad (3.2)$$

where a_x , a_y and a_z are the acceleration measured along the x, y and z axis respectively.

Heading or orientation (yaw) can be calculated from the magnetometer data (m_x, m_y, m_z) if it is available. It is impossible to calculate the value for yaw using the accelerometers only as the rotation around the horizontal plane is not captured. In order to measure yaw the system needs to use a gyroscope and/or magnetometer (Y. Wang et al., 2018). The gyroscope provides the values of angular velocities along the 3-axes. Using this, it can obtain the change in pitch, roll and yaw by integrating these values over time, but to calculate absolute values of these angles it needs reference data (or starting absolute value). This can be obtained from the accelerometer for roll and pitch, but is obtained from the magnetometer for yaw. For calculating yaw, the data from the IMU uses magnetometer data as reference and then integrates the gyroscope data over time.

The magnetometer can find the orientation of an object using the earth's magnetic field, similar to a compass, in terms of yaw when combined with the data from the accelerometer. Integrated magnetometer and accelerometer data provides yaw value based on the following equations (Nurhakim et al., 2019):

$$\text{mag}_x = m_x \cos(\text{pitch}) + m_y \sin(\text{roll}) \sin(\text{pitch}) + m_z \cos(\text{roll}) \sin(\text{pitch}) \quad (3.3)$$

$$\text{mag}_y = m_y \cos(\text{roll}) - m_z \sin(\text{roll}) \quad (3.4)$$

$$\text{yaw} = \text{atan} \left(\frac{-\text{mag}_y}{\text{mag}_x} \right) \quad (3.5)$$

In this case, m_x , m_y and m_z are the magnetic field strength in x, y and z direction respectively. Roll and pitch are calculated from equations 3.1 and 3.2. From the above equations. It can be concluded that:

- If $m_x, m_y > 0$, then orientation is $(90 - \text{atan} \left(\frac{m_x}{m_y} \right) * 180/\pi)^\circ$
- If $m_y < 0$, then orientation is $\left(-\text{atan} \left(\frac{m_x}{m_y} \right) * 180/\pi \right)^\circ$
- If $m_y = 0$ and $m_x < 0$, then orientation is 180°
- If $m_y = 0$ and $m_x > 0$, then orientation is 0°

In the results the orientation/heading only depends on the accelerometer and magnetometer measurements. Since roll and pitch are valid if the system is not under acceleration (i.e. moving forward), then the values will be effected over the period of acceleration from the movement, thus this drawbacks leads to a limitation of the magnetometer performance. However the gyroscope is only able to measure relative values or angular velocity (O'connor et al., 1976). For measuring angles using a gyroscope sensor, errors accumulate resulting in insufficient data calculation. Ismail et al. (2018) proposed eight different methods for the integral calculation of the gyroscope sensor (Ismail et al., 2018).

This measurement is affected by the drift of the gyroscope, which will be addressed in chapter 4. For measuring absolute values of angular velocity, a combination of accelerometer and magnetometer is required. Based on the various drawbacks in all the systems, all three systems need to be used in conjunction with each other to provide reliable solutions.

3.3 IMU for positioning and orientation in UAV system

IMUs are a main component of the Inertial Navigation System (INS) used in UAVs/Drone. The data collected by an IMU is processed by the system to track position through Dead Reckoning (DR) (Loewy, 2003). DR calculates current position according to the previously determined position and the relative changes observed through the IMU over time. Common applications for IMUs include control and stabilisation, navigation and correction, measurement and testing, unmanned systems control, and mobile mapping (Noureldin, 2013). If the initial pose is known, and if perfect models for the IMU exist, the process illustrated would lead to perfect position estimation. In practice, however, the inertial measurements are noisy and biased, as will be discussed in more detail in the following sections. Because of this, the integration steps from angular velocity to rotation and from acceleration to position will introduce the errors in the sensors.

To measure the position and orientation of a device (e.g. drone) using an IMU, first the sensor orientation is provided by the gyroscope integration. The subtraction of earth's gravity, which is determined by the orientation of the sensor and double integration of the accelerometer present the sensor position (Hoflinger et al., 2013) (Kok et al., 2017). Figure 3.4 illustrate Dead Reckoning method which is the process of integrating the measurements from inertial sensors (accelerometer and the gyroscope) to obtain position and orientation information.

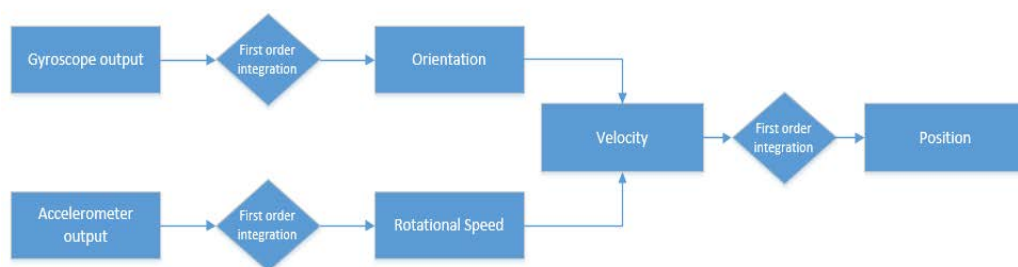


Figure 3.4 Dead Reckoning method based on integrated accelerometer and the gyroscope to find position and orientation

To calculate position and orientation from the IMU, acceleration and angular velocity is integrated over time. This can be done using the accelerometers to calculate the velocity by incorporating the measured acceleration. Then, by adding the velocity, the position can be measured from a reference point of x, y, z . This method is beneficial when the estimator is for a short period of time because uncertainty accumulates or grows exponentially over time (Kok et al., 2017).

In order to define the correct position based on time (t) and velocity (V) in an INS, the data generated by an IMU is processed via a computer, and these physical properties can implement Dead Reckoning. For example, if a drone is flying east at 10 m/s, it can be concluded that its new location is 10 metres east of its initial position after an interval 1 second. Distance is the speed travelled multiplied by the amount of time travelled. Given the right information and using this basic formula, it can be determined how far the drone has travelled. Combining this method to a system of maps can show where a drone is on the map similar to GNSS, but without the need to be connected to or in communication with any outside systems. In order to use the

Dead Reckoning method, basic kinematic formulas are used. t_0 denotes the time at position X_0 and velocity V_0 . The new position X_1 can be calculated as follows:

$$X_1 = X_0 + V_0(t_1 - t_0) \quad (3.6)$$

In case of having acceleration, the formulas below will apply, where A_0 denotes acceleration at t_0 :

$$V_1 = V_0 + (t_1 - t_0)A_0 \quad (3.7)$$

$$X_1 = \frac{1}{2} A_0 (t_1 - t_0)^2 + V_0(t_1 - t_0) + X_0 \quad (3.8)$$

(Jacky et al., 2018) proposed a solution from the estimated accelerometer and gyroscope calibration parameters which deliver a more accurate Dead Reckoning solution than the popular multi-position calibration method by recovering the gyroscope scale error and other systematic errors.

The data received from an IMU needs to be processed in order to calculate the changes in the drone's positions and orientations. In an effort to reduce the effect of noise from the environment and sensors and reduce drift, methods need to be employed an adapted to help eliminate and reduce these effects. These may include different types of filtering methods such as Kalman or complementary filters based on established methodology used in drones (Huang et al., 2015) (Yuan, Yu, Zhang, Wang, & Liu, 2015).

3.4 Errors, initialisation and compensation

The data received from an IMU needs to be processed in order to calculate the change in the drone's position and orientation. Specifically, this means that there are some errors which occur and accumulate, and their effects need to be propagated in presented data.

The IMU starts collecting data through its sensors, namely, accelerometer, gyroscope and magnetometer, to calculate the roll, pitch, and yaw. This data assists in obtaining

the movement distance in each time interval. This information supports the drone in avoiding obstacles. A great challenge regarding utilising IMU is related to sensors' noise and gyroscopic drift. It has the most adverse impact, which exponentially increases over long distances. IMU has an unlimited drift in the velocity, position, and altitude caused by a gyroscope in long distance.

3.4.1 Initialisation and calibration of IMU

To reduce environmental (compensation) and sensor noise, alongside drifting over time which will affect the IMU observed data, calibration of the IMU is important. A general method for IMU calibration is performed by putting it in a static and still position until roll, pitch, and yaw values become stabilised (D. Lee et al., 2011). Then each axis sensitivity has adjustment values applied by measuring the stable conditions over time and calculating the necessary corrections.

When an IMU is configured for capturing data continuously, it needs to be calibrated to initialise for capturing. Accelerometer calibration only needs to be done once. During calibration, the hardware must be stable. Magnetometer calibration should be done in the final installation location with everything powered and running. Any changes in the magnetic or electrical environment could affect the calibration, and it would require performing a new magnetometer calibration if these conditions change. For gyroscope calibration the gyroscope biases need to be addressed. Again, the IMU needs to be motionless, but not necessarily level. Additionally, gyro bias is highly sensitive to temperature, therefore calibrating the gyros is required every time the sensor is used rather than storing and using a static set of gyro biases (Hemanth et al., 2012).

Regarding calibration for specific types of IMU, the MPU 9250 used in this research is first calibrated in the factory to acquire values for accelerometer, gyroscope and magnetometer in the triple axis (x,y,z), which can then be extracted. The MPU 9250 used in this research has its own specific calibration and initialisation. Firstly, factory calibration values for the accelerometer, gyroscope and magnetometer in the triple axis (x,y,z) are extracted. Then, each axis sensitivity value is adjusted using a loop and wait process until the numbers stabilise. Using a sufficient delay in loop simulation is

essential as otherwise the sensors can never reach stabilised values. For the specific IMU used in this research sensor calibration takes approximately 8 seconds.

3.4.2 Compensation and information fusion

An essential element of the design of autonomous systems is sensor fusion. This can be done by integrating two or more data sources. This allows for consistent information with an increase in accuracy and reliability which is not seen within a single data source. In order for autonomous systems to be successful in interacting with their surroundings, four main areas are necessary. These are known as Sense, Perceive, Plan and Act. Sensors collect information from the system and the environment, representing the Sense area. The Perceive step provides information from previously sensed data. Planning determines what it needs to accomplish and finds a path to allow it to do so. Finally, Act calculates the actions needed for the system to track the path. This step determines the actions of the controller and the control system.

The perceive step has two different responsibilities. Self-awareness, referred to as localisation or positioning and is where sensor fusion is integrated. The localisation and positioning of a system, while simultaneously detecting and tracking other objects are actions undertaken by sensor fusion. This results in the system working with data with less noise and uncertainty, alongside fewer deviations. For example, a single accelerometer placed on a table only measuring the acceleration as a result of gravity. A perfect sensor output would measure a constant 9.81 m/s^2 , however the actual measurement is still noisy. Noise depends on the quality of the sensor and is usually randomly distributed, so it cannot be removed through calibration alone.

To reduce the noise an additional accelerometer can be added and by averaging these two readings the noise will be reduced. Fusing sensors together to reduce the combined noise is only effective when the noise is not correlated with the sensor. Fusing identical sensors will result in half of the noise of a single sensor. The averaging function is the core of this fusion algorithm. For example, to measure the direction of an IMU which is facing relative to North, the magnetometer in the system could be used to measure the deviation of the angle from magnetic North. However, this sensor measurement will be still noisy due to noise or interference.

To reduce noise a second magnetometer can be added. However, in this situation the noise is coming from the moving magnetic fields, created by the system's electronics. This implies that the correlated noise source will affect every magnetometer and will not remove noise through the averaging. To solve this problem there are two options, one being to move the sensors away from the external interference, or to filter the measurement through some forms of filtering methods. The second option is to fuse the magnetometer with the angular rates measures by the gyroscope. The gyro will be noisy as well, however the true values should be complementary. Using two different sensor types may reduce the correlation between the different sensor noises, and so be used to correct each other. If a change is measured in the magnetic field by the magnetometer, the gyro can be used to determine whether the rotation is from physical movement of the drone or from noise (MathWorks, 2020).

Compensation based on the earth rotation over time and the factors caused by the effect of latitude and elevation, need to be applied to the gyroscopes and accelerometers (Stephenson, 2003). Considering these compensations are necessary to obtain accurate data. Generally, observed data consists of both the real data and compensations. These compensations must be applied by considering them as default values. The major gyroscope compensation is the average of the angular velocity of the rotation of the earth. It can be calculated from the following formula based on earth's rotation which moves approximately 360 degrees per 24 hours. Velocity (rad/s) equals movement caused by rotation (m) over time in second (s):

$$V = \frac{\Delta d}{\Delta t} = 7.26e^{-5} \text{rad. s}^{-1} \quad (3.9)$$

The accelerometer compensation is based on the global velocity (nominally (0, 0, 9.8) m/s⁻²). The three components are (ax, ay, az) and their direction state 9.8 ms⁻² in the vertical direction.

Generally, roll and pitch are calculated by the gyroscope and accelerometer. The gyroscope can respond quickly to change, however, depending on its sensitivity it will

create drift along these rotational axis by accumulating errors over time. Because of this and the dynamic sensors noise from the three components of the IMU influencing its output, it is therefore required that an appropriate filter is used based on the nature of generated data. In most cases, to address drift issues of the gyro, using a filter such as the KF and considering bias and compensation are recommended for data fusion, however high accuracy sensor fusion, and constant sampling rate must be taken into account (Smyth et al., 2007). That contrasts with the sampling rate for the synchronisation of the IMU data and capturing device, such as the low frequency capturing rate for an image frame by camera.

3.5 Filtering

To reduce the effect of noise from the environment and sensors, and to reduce drift, filtering methods need to be investigated and adapted. These may include different types of filtering methods such as the Kalman Filter (KF), the Extended Kalman filter (EKF), the Complementary Filter (CF), the Particle Filter (PF) and the Artificial Intelligence (AI) based on stablished methodology used in drones (Noureldin, 2013). However, while there are several filtering methods to address the stated issue of IMU, this research focused on implementing the KF in order to achieve a solution. It is worth mentioning the state of art to solve this problem is based on Artificial Intelligence namely deep Neural Networks (NN). Since applying NN as a deep learning method requires a very large data set and accurate ground truth, an insufficiency in data meant it was not possible to use NN within this research (Brossard et al., 2020).

KF uses both measurements from the accelerometer and gyroscope to estimate the current pose and to reduce drifts and errors (Zhang et al., 2014). (Gui et al., 2015) proposed a method using the CF algorithm which uses a low-pass filter and a high-pass filter to deal with the data from accelerometer and gyroscope, while the KF takes the tilting angle and gyroscope bias as system states, combining the angle derived from the accelerometer to estimate the tilting angle.

EKF is a special case of the KF that is used for nonlinear systems (Alatise et al., 2017). EKF is used to estimate the drone position and orientation by employing the prediction and correction from a nonlinear system model. EKF was designed to correct each sensor error by fusing the inertial and vision data together to obtain accurate orientation and position.

KF is designed to predict the future behaviour of data based on analysing the previous existing values, whereas CF works based on linear computation. The recursive functionality of KF makes it superior when compared to CF due to its low time and processing power requirements. This characteristic of KF makes it a preferred method as its algorithm takes less time and processing power on a drone. KF is one of the more common methods, and a key attribute is that a mathematical model of the system is already built into the filter. Another filtering method such as Particle Filter (PF) uses a suboptimal observer that can estimate the states of a nonlinear non-Gaussian system (Seong-hoon et al., 2008).

Although there are several sensor fusion algorithms, at their core every one of them follows a similar procedure. That is, they initialise attitude either by setting the values manually or using the initial results of the magnetometer and accelerometer, and over time used the direction of the magnetometer field and gravity to slowly correct for the drift in the gyro. For example, Mahony orientation filter method uses a proportional and integral controller to correct the gyroscope bias, whereas the Madgwick filter method uses only a proportional controller (Ludwig et al., 2018). Both approaches use a quaternion representation, which is a four-dimensional complex number representing the orientation of an object.

3.5.1 Principal of filtering

The data received from an IMU needs to be processed in order to calculate the changes in the drone's positions and orientations. To reduce the effect of noise from the environment and sensors, and to reduce drift, methods need to be employed and adapted to help eliminate and reduce these effects. These may include different types of filtering methods such as Kalman or complementary filters based on established methodology used in drones (Yuan, Yu, Zhang, Wang, & Liu, 2015).

3.5.2 Complementary filtering

Complementary Filter is usually a low pass/high pass filter pair (Higgins, 1975). The purpose of using CF is to combine accelerometer and gyroscope values to estimate IMU orientation. Both gyroscope and accelerometer can indicate IMU angles, an accelerometer generates data which are reliable in low frequency signals, whereas a gyroscope reports data which are more accurate in higher frequency ranges. In order to smooth the accelerometer data, a low-pass filter is required, while a high-pass filter is needed to filter the gyroscope data. Complementary in this sense means that the system combines the two measurements in a way that complements each other. In other words, it takes some part of one measurement and adds the complementary part of the other so that the sum of the two parts is one measurement. Accelerometer measurement is passed through low-pass filter $G(s)$ while the measurement passed through gyro is high-pass filter $([1 - G(s)])$.

Since adding these two filters together equals one, then they are complimentary of each other, so the resulting sum of the low pass and high pass filter is always equal to one, and this means at low frequencies the accelerometer data (acc) has a higher determining factor over gyroscope values, while conversely the gyroscope values (gyro) at high frequencies will influence the final value more than the values from the accelerometer. A mathematical form of this complementary filter can be written as:

$$\begin{aligned} \text{angle} &= (1 - \alpha) * (\text{angle} + \text{gyro} * dt) + (\alpha)(\text{acc}) \\ 0 &\leq \alpha \leq 1 \end{aligned} \tag{3.10}$$

where α denotes a time constant which is between 0 and 1. It defines the boundary where the accelerometer readings stop and the gyroscope readings take over and vice-versa. Influence is determined depending on the frequency of movement:

- Lower frequency results in the angle from accelerometer having a higher influence.
- High frequency results in the angle from gyroscope having a higher influence.

The complementary filter consists of both low and high pass filter, and due to the fact that it is easier to implement, it was used to obtain precise data. KF requires less memory by using previously existing data than compared with the complementary filter, and because of this advantage this study will focus on using the KF.

3.5.3 Kalman Filtering

KF are often used to optimally estimate the internal states of a system in the presence of uncertain and indirect measurements (Gede, 2011). KF for INS combines different measurements considering estimated errors to produce a trajectory including time, position and attitude. KF describes clearly how each state can be affected by the previous state and how measurements depends on each state. Figure 3.5 illustrates the KF estimation of the current state by calculating the predicted value of the state combined with the factor of measurement and predicted value.

$$\boxed{\text{The estimate of the current state}} = \boxed{\text{Predicted value of the current state}} + \boxed{\text{Factor}} \times \left(\boxed{\text{Measurement}} - \boxed{\text{Predicted value of the current state}} \right)$$

Figure 3.5 KF state estimation

In order to design a KF for a system, three major definitions are needed. A KF combines these measurements and predicts the optimal estimate of the IMU position and velocity. Generally, the three components are defined as 1) State Update, 2) Time Update and 3) Measurement Update:

State Update: KF are used to estimate states based on linear dynamical systems in state space format.

The process model defines the evolution of the state from time $k - 1$ to time k as:

$$x_k = Ax_{k-1} + Bu_{k-1} \quad (3.11)$$

Where A the state transition matrix is applied to the previous state vector x_{k-1} and B is the control input matrix applied to the control vector u_{k-1} .

In other words both A and B are coefficient values obtained by KF, where as x_k and x_{k-1} respectively are the values of interest in states k and $k - 1$, and u_k is control system in states (state $k - 1$ and k denote Kalman gain at time stamp $t - 1$ and t).

Time update: This is simply the difference in time between one update and the next and is defined as:

$$\Delta_t = t_{k+1} - t_k \quad (3.12)$$

Measurement update: The process model is paired with the measurement model that describes the relationship between the state and the measurement at the current time step k as:

$$K = P_k H^T (H P_k H^T + R)^{-1} \quad (3.13)$$

The measurement update equation (3.13) calculates the Kalman gain K , which is used to update the state estimate x_k with the measurement at time step k . The measurement update involves the state covariance matrix P , the observation matrix H , and the process covariance matrix R , which describes the noise in the system. The equation calculates the Kalman gain as the product of the state covariance matrix P_k and the transpose of the observation matrix H , divided by the sum of the product of the observation matrix H and the state covariance matrix P_k , multiplied by the transpose of H , and the process covariance matrix R .

R denotes a 3x3 matrix for 3D purposes and 2x2 matrixes for 2D such as:

$$R_{\text{acc}} = \begin{bmatrix} \Delta_{\text{ax}}^2 & 0 \\ 0 & \Delta_{\text{ay}}^2 \end{bmatrix}$$

$$R_{\text{gyro}} = \begin{bmatrix} \Delta_{\text{gx}}^2 & 0 \\ 0 & \Delta_{\text{gy}}^2 \end{bmatrix}$$

P represents the state covariant matrix, H is the observation Matrix, and Q is the process covariance matrix which describe the noise in the system and is obtained from FR_vF^T when:

$$F = \frac{\Delta x}{\Delta v} \quad (3.14)$$

where x is the desired output and v is device noise. Generally, Δ indicates difference values between stated $k + 1$ and state k.

The KF is capable of combining multiple inputs from various sensors and not only generates an approximation of current state of a system, but also is able to predict forthcoming status of the system. Generally speaking the KF is a statistical approach which integrates data of statistical nature of system errors with variables of a system dynamics to estimate state of a system. Velocity and position are main variables in any navigation system. In order to obtain minimum error variance in estimation of system status, Kalman gain is used which a weighing function is based on optimised KF.

A limitation is normally based on linear motion and non-linear motion. In the Extended Kalman Filter (EKF), the state transition and observation models do not need to be linear functions of the state, therefore it makes use of a nonlinear state space model. However, it may instead be differentiable functions. EKFs compute filtering estimates in terms of the conditional probability distribution. EKF can be interpreted as Gauss-Newton optimisation of the filtering problem using only one iteration with a step length of one (Kok et al., 2017). In order to deal with nonlinear models efficiently in navigation systems, the EKF is introduced, due to the fact that it is computationally optimised comparing with other nonlinear filtering method e.g. Point-Mass Filters and Particle Filter (Alatise et al., 2017).

3.6 Chapter Summary

Microelectromechanical system (MEMS) inertial sensors have become widely available due to their small size and low cost. These IMUs perform at high sampling rates and can be integrated to obtain position and orientation information. These estimates are accurate on a short time scale, but suffer from integration drift over longer

time scales (accumulating error). To overcome this issue, inertial sensors are typically combined with additional sensors and models. KF is a suitable candidate for sensor integration.

Some advantages of the KF over the Complementary filter:

1. **Increased Accuracy:** The KF is a more sophisticated algorithm that incorporates both the measurement data and the state estimate to produce a more accurate result. This results in a more accurate estimation of the orientation and position of the IMU.
2. **Adaptability:** The KF is adaptable to changing conditions, such as changes in the motion or environment. This allows it to be more robust and effective in removing gyro drift in complex environment
3. **Handling Uncertainty:** The KF is capable of handling uncertainty in the measurement data, which is important in removing gyro drift in IMU. The complementary filter, on the other hand, assumes that the measurement data is always accurate, which is not always the case in real-world scenarios.
4. **State Estimation:** The KF provides a continuous state estimation, which can be useful for navigation purposes. The complementary filter, on the other hand, provides only a filtered output, which may not be as useful for navigation purposes.

In conclusion, the KF is a more advanced and sophisticated algorithm for removing gyro drift in IMU compared to the complementary filter. However, the choice of algorithm ultimately depends on the specific requirements and constraints of the application.

4 IMU FILTERING METHODOLOGY AND PROTOTYPE

4.1 Introduction

As discussed in the previous chapter, for this research an IMU is ideal for tracking the state of a drone over a short period of time, as well as measuring changes in orientation. Based on a previous study in (Nazemi et al., 2021), the basic position or first IMU measurement is realised as soon as the capturing device detects a manmade marker and utilises this as the starting point. Through the detection of the manmade markers, global coordinate values of the drone location are obtained. Based on this initial information, the IMU can then estimate the changes in orientation and position, and then be used in the drone control.

The method proposed in this research focuses on calculating the orientation and position after this starting point using data from a low cost IMU commonly used in UAV systems. In calculating this information reliably, a high level of positioning accuracy is needed to control the drone and process the data. This means that the noise and exponential accumulation of errors (such as gyro drift) needs to be processed efficiently to convert the raw collected data to more accurate information in order to provide the orientation, velocity and distance. To address this problem, the IMU data collection and filtering will be outlined in the following sections. The prototype designed for testing these values will also be described.

4.2 Filtering Implementation

Various methods of filtering may be employed, as discussed in section 3.5. Since the drift and noise in this system are stochastic (not predictable), accumulative, and not deterministic, this research focused on designing a KF for this specific case. A deterministic system is a system in which no randomness is involved in the development of future states of the system. A stochastic system has a random probability distribution or pattern that may be analysed statistically, but cannot be predicted precisely. An accumulative system consist of developing data over time in an incremental pattern.

The KF is a statistical method that combines the knowledge of the statistical nature of system errors with a knowledge of system dynamics, as represented by a state model. The KF provides an estimate of the state of a system to predict the future state of the system. Any variable can be included in the states. In the navigation system, they are usually concerned with position and velocity. The state estimate is obtained by using a weighting function called the Kalman gain (K), which is optimised to produce a minimum error variance.

As stated previously (equations 3.1 to 3.5), in the first implementation for this system and to avoid the usage of a filter, roll and pitch are obtained respectively from Angle_x (ax) and Angle_y (ay) from the accelerometer. However, experimental results demonstrate it is impossible to calculate the value for yaw using the accelerometers only as the rotation around the horizontal plane is not captured. The drone heading is primarily provided by the magnetometer, but as highlighted in section 3.2.3, it can be supplemented by other sensors and it needs accurate roll and pitch data to calculate yaw (Baranek et al., 2012).

Based on its quick response to change, the changes in roll and pitch are calculated by the gyroscope. The gyroscope provides the values of angular velocities along the 3-axes. Gyro sensitivity leads to drift being generated along these rotational axes by accumulation of errors over time. To avoid drift in the gyroscope and to obtain an accurate orientation, a KF is used to integrate two vulnerable sensors, the accelerometer and the gyroscope.

In addition, the reasons behind filtering data in this research is to overcome environmental (compensation) and sensor noise, alongside sensors drifting over time, which affect the IMU data observed. By employing a filter, it allows for the processing and elimination of such adverse effects. Within this research, the filter was used primarily for the roll and pitch data, not the yaw/magnetometer data. However, based on equation 3.5, the filtered roll and pitch data is still critical for the estimation of the orientation using the magnetometer.

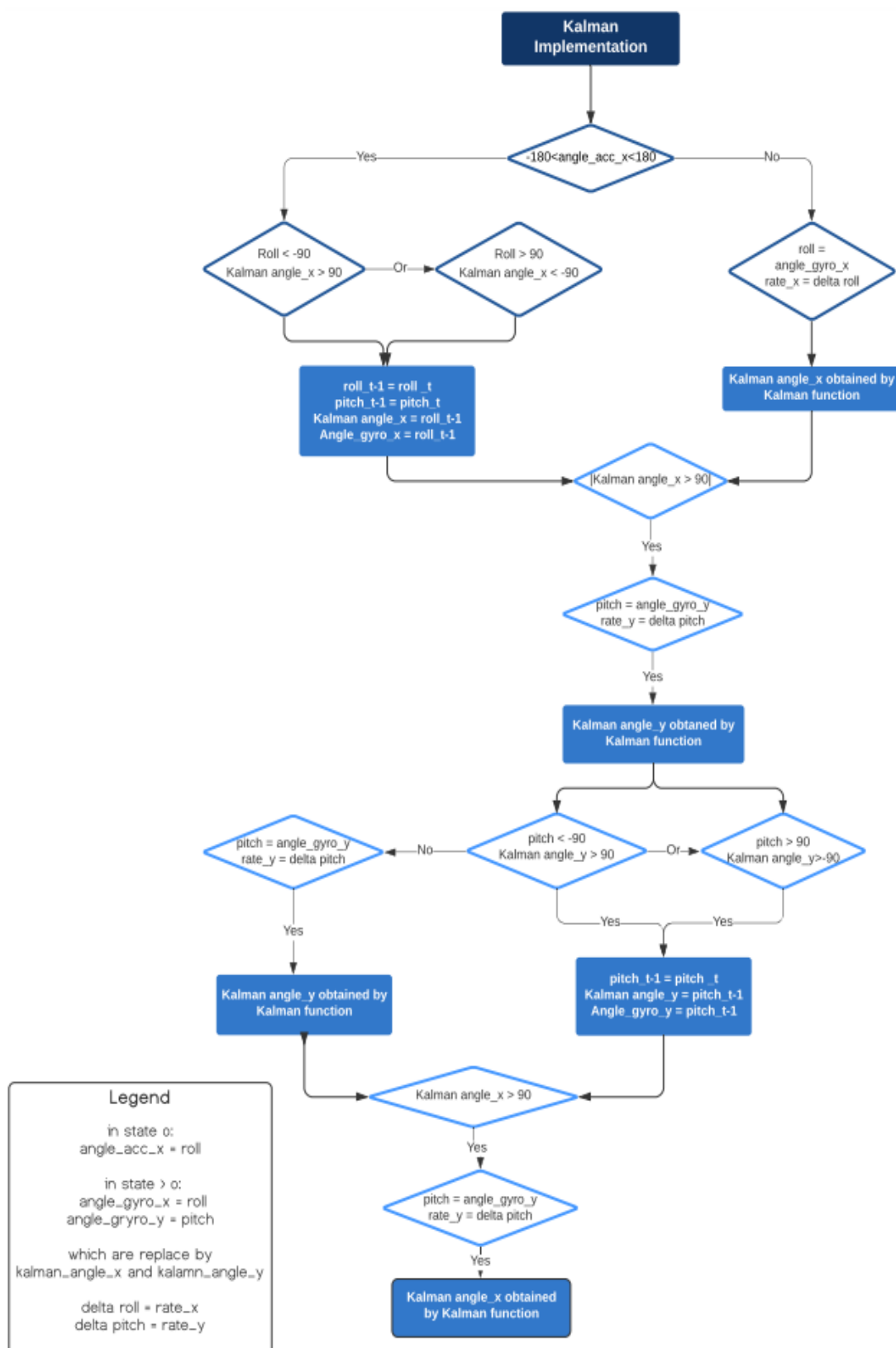


Figure 4.1 Kalamn Filter (KF) Implementation.

In order to design a KF for a system, three major components need to be defined. Generally, the three components to be defined are 1) State Update, 2) Time Update and 3) Measurement Update, described in equations 3.11, 3.12, and 3.13. The KF combines measurements based on these equations, and uses them to predict the optimal estimate of IMU position and velocity/heading.

Figure 4.1 is an overview block diagram for filtering implementation in this research which illustrate state update, measurement update and time update. Each steps are explained in more detailed in the remaining parts of this section.

State zero: State zero in the overview block diagram is indicated by the top most decision box. Using the gyro measurements, the change in pitch, roll and yaw can be obtained by integrating these values over time. However, in order to calculate the absolute values of these angles, reference data is needed. This can be obtained from the accelerometer for roll and pitch:

$$\text{angle}_{\text{acc}_x} = \text{roll} \quad (4.1)$$

$$\text{angle}_{\text{acc}_y} = \text{pitch} \quad (4.2)$$

For calculating yaw, the data from the IMU uses the magnetometer data as reference and then integrates the gyro data over time. The $\text{angle}_{\text{acc}_x}$ and $\text{angle}_{\text{acc}_y}$ are the angles calculated from the accelerometer, and are not the accelerometer raw value (a_x, a_y, a_z). The state vector for this system is a 2D vector. The Figure description is focused on the application of defining $\text{angle}_{\text{acc}_x}$, but can also be employed for $\text{angle}_{\text{acc}_y}$. The angle has the following properties:

$$-180 < \text{angle}_{\text{acc}_x} < 180 \quad (4.3)$$

$$\text{angle}_{\text{acc}_x} = \text{roll}$$

$$\text{roll} = \text{atan} \left(\frac{a_y}{\sqrt{a_x^2 + a_z^2}} \right)$$

State Update: KF are used to estimate states based on linear dynamical systems in state space format.

The process model defines the evolution of the state from time $k - 1$ to time k as:

$$x_k = Ax_{k-1} + Bu_{k-1}$$

In other words, both A and B are coefficient values obtained by KF, where as x_k and x_{k-1} respectively are the values of interest in states k and $k - 1$, and denote Kalman gain at time stamp $t - 1$. u_k is the control system in states.

Kalman gain is the most significant parameter for the filter, which is represented by a 2D vector and is denoted by $[K_t, K_{t-1}]$. This represents for this research $[K_{\text{angle}_{x_t}}, K_{\text{angle}_{x_{t-1}}}]$ or $[K_{\text{angle}_{y_t}}, K_{\text{angle}_{y_{t-1}}}]$.

Matrix A is the state transition matrix as applied to the previous state vector x_{k-1} and B is the control input matrix applied to the control vector u_{k-1} and u_k is control system in states. In the overview block diagram, x in equation 3.11 translates as $\text{angle}_{\text{gyro}_x}$ and $\text{angle}_{\text{gyro}_y}$ respectively, to represent the angle of the drone around the x -axis and y -axis (as illustrated in Figure 3.3 and section 3.2.5), which is defined as the system description in the Kalman design for this study.

The state vector for this system is a 2D vector which contains: $\begin{bmatrix} \text{angle} \\ \text{bias}_{\text{gyro}} \end{bmatrix}$

The angle and bias refer to the angle x and y for the gyro:

$$\begin{bmatrix} \text{angle}_{\text{gyro}_x} \\ \text{bias}_{\text{gyro}_x} \end{bmatrix} \text{ and } \begin{bmatrix} \text{angle}_{\text{gyro}_y} \\ \text{bias}_{\text{gyro}_y} \end{bmatrix}.$$

Bias, previously described in section 3.4, is used when the system must compensate for the measurement value not starting from zero. For the specific IMU used in this research, MPU 9250, the calibration values are as follow and were obtained after approximately 8 seconds.

Accelerometer bias represent by (ax, ay, az) and obtained $(-86.91, -37.84, -11.17)$. Gyro bias represent by (gx, gy, gz) obtained these values $(1.50, -0.50, 0.70)$ [deg/s] (TDK, 2021).

Time update: This is simply the difference in time between one update and the next and is defined as: $\Delta_t = t_{k+1} - t_k$

The IMU has three different sensors with different sampling rates. The different sampling frequencies need to be combined through synchronisation. To sync two devices with different frequencies, the data from the higher frequency device must be collected in a specific time interval. The rate of sampling of the higher frequency device to the lower frequency device defines this time interval.

The IMU utilised in this research is a MPU9250, which includes a gyroscope and accelerometer. The accelerometer frequency is set to 260 Hz, and the gyroscope is set to 256 Hz. The capturing device frequency is calculated based on the timestamps and number of samples. Considering n is the number of samples, $t = \{t_0, t_1, \dots, t_n\}$ is the sampling period and t_0 to t_n is the time interval, then the system period or Δ_t is calculated by:

$$\Delta_t = t_n - t_0 \quad (4.4)$$

To calculate the frequency, which is equal to sampling rate, the number of samples need to be divided by the sampling period:

$$\text{Frequency} = \text{sampling rate} = \frac{n}{\Delta_t} \quad (4.5)$$

To sync two devices with different frequency the data from high frequency device must be collected in the sampling interval defined by:

$$\text{sampling time interval} = \frac{\text{high frequency device}}{\text{low frequency device}} \quad (4.6)$$

As mentioned in this example, the sampling time interval can be calculated by the accelerometer frequency divided by the magnetometer frequency, therefore for the magnetometer and accelerometer the sampling time interval is 4. This sampling time interval is calculated based on the accelerometer frequency being the high frequency sensor, and it in turn is used to calculate the optimised sampling time interval between

accelerometer and gyroscope. The frequency of the gyro in full power mode (3.2 mA) is 1000 Hz for Output Data Rate (ODR), however on average it operates at 256Hz.

The sampling time interval between the accelerometer and gyroscope is obtained from dividing the gyroscope frequency by the accelerometer frequency, which is equal to 32 for the IMU used in this research, but may vary based on the IMU specifications.

Measurement update: As stated in section 3.5.3 the measurement update formula in the KF is given by: $K = P_k H^T (H P_k H^T + R)^{-1}$

In this equation, K is the Kalman Gain, P_k is the state covariance matrix, H is the observation matrix, and R is the measurement covariance matrix. The Kalman Gain is used to weigh the importance of the predicted state and the measurement, with the measurement being more reliable, the weighting will be higher and vice versa. The state covariance matrix P_k and the measurement covariance matrix R , both describe the uncertainty in the system. The observation matrix H describes the relationship between the state and measurement.

In general terms x indicates the vector of interested parameter in any system. For example, in an Inertial Navigation (INS) system. This vector indicates position and the parameters are velocity and heading per time interval, the x vector determine by at 2x1 matrix as $\begin{bmatrix} \text{velocity} \\ \text{heading} \end{bmatrix}$. K is Kalman gain. u is the vector of controlling factor in state. x_k is the position in the state at time t_k , x_{k-1} is the position in previous state and u_k is velocity of the state. R denotes a 3x3 matrix for 3D purposes and 2x2 matrixes for 2D such as:

$$R_{\text{acc}} = \begin{bmatrix} \Delta_{\text{ax}}^2 & 0 \\ 0 & \Delta_{\text{ay}}^2 \end{bmatrix} \quad (4.7)$$

$$R_{\text{gyro}} = \begin{bmatrix} \Delta_{\text{gx}}^2 & 0 \\ 0 & \Delta_{\text{gy}}^2 \end{bmatrix}$$

P represents the state covariant matrix:

$$P = \begin{bmatrix} P_{00} & P_{01} \\ P_{10} & P_{11} \end{bmatrix} \quad (4.8)$$

H is the observation Matrix:

$$H = [1 \ 0]$$

Q is the process covariance matrix which describe the noise in the system and is obtained from FR_vF^t .

$$F = \frac{\Delta_x}{\Delta_v}$$

where x is desired output and v is device noise. Generally, Δ indicates difference value between stated $k + 1$ and state k .

To design a KF in this system based on the 2D purpose, the Kalman gain (which minimizes the estimate variance) is a 2x1 vector represent by $[K_t, K_{t-1}]$ that is satisfied in the following equations:

$$\text{Angle}_k = \text{Angle}_{k-1} + (K_{t-1} * \Delta_{\text{angle}}) \quad (4.9)$$

$$\text{bias}_k = \text{bias}_{k-1} + (K_t * \Delta_{\text{angle}}) \quad (4.10)$$

In addition, the error covariance matrix for state matrix x is a 2D matrix which is denoted as P_t , and is calculated by:

$$P_t = \begin{bmatrix} P_{00_t} & P_{01_t} \\ P_{10_t} & P_{11_t} \end{bmatrix} \quad (4.11)$$

$$P_{00_t} = P_{00_{t-1}} + \Delta_t * (\Delta_t * P_{11_t} - P_{01_t} - P_{10_t} + Q_{\text{angle}}) \quad (4.12)$$

$$P_{01_t} = (\Delta_t * P_{11_t}) - P_{01_{t-1}}$$

$$P_{10_t} = (\Delta_t * P_{11_t}) - P_{10_{t-1}}$$

$$P_{11_t} = (Q_{\text{bias}} * \Delta_t) + P_{11_{t-1}}$$

After using the KF, the error covariance matrix can be updated as the following:

$$P_{00_t} = (K_{t-1} * P_{00_t}) - P_{00_{t-1}} \quad (4.13)$$

$$P_{01_t} = (K_{t-1} * P_{01_t}) - P_{01_{t-1}}$$

$$P_{10_t} = (K_{t-1} * P_{10_t}) - P_{10_{t-1}}$$

$$P_{11_t} = (K_{t-1} * P_{11_t}) - P_{11_{t-1}}$$

The process noise variance for the accelerometer (Q_{angle}), process noise variance for the gyro bias (Q_{gyroBias}) and variance of the measurement noise (R_{measure}) is predefined in the factory. So based on this factory setting for the IMU used in this research, it is assumed that Q_{angle} is set to 0.001 and Q_{gyrobias} is set to 0.003 with R_{measure} set to 0.03 in this case. From these assumed values, here S is the estimated error which is satisfied in the following equation and the Kalman gain can be obtained by:

$$K_{t-1} = \frac{C_{00t}}{S} \quad (4.14)$$

$$K_t = \frac{C_{10t}}{S} \quad (4.15)$$

$$S = C_{00t} + R_{\text{measure}} \quad (4.16)$$

$$\text{angle} = \text{angle} + (K_{t-1} * y) \quad (4.17)$$

$$\text{bias} = \text{bias} + (K_t * y) \quad (4.18)$$

Here y is angle difference (new angle – angle) and in equation 4.11 y can be translated as either:

- Assuming Kalman represent by Kalman x then y is:

$$y = \Delta_{\text{anglegyro}_x} = \Delta_{\text{roll}} \quad (4.19)$$

- Assuming Kalman represent by Kalman y then y is:

$$y = \Delta_{\text{anglegyro}_y} = \Delta_{\text{pitch}} \quad (4.20)$$

If the filter is for roll or pitch, as similarly shown in equation 4.10, bias can be translated as 4.21 and 4.22 (depending on if the value is being applied to roll or pitch).

For roll the bias is defined as:

$$\text{bias} = \text{bias}_{\text{gyro}_x} \quad (4.21)$$

For pitch, the bias is defined as:

$$\text{bias} = \text{bias}_{\text{gyro}_y} \quad (4.22)$$

In equation 4.11, angle can be represented by (depending if the value is being applied to roll or pitch):

$$\text{angle} = \text{angle}_{\text{gyro}_x} \quad (4.23)$$

For pitch, the angle is defined as:

$$\text{angle} = \text{angle}_{\text{gyro}_y} \quad (4.24)$$

As the state estimate is obtained by using the Kalman gain K as a weighting function, this will then provide a more accurate Kalman gain calculation, resulting in access to more robust system vector values.

4.3 System Prototype

The following section briefly explains the applied designed system using this research for drone navigation in underground mining, as mentioned in this chapter's introduction. The IMU starts to process data as soon as the capturing device detects the manmade marker sign at the starting point and the calibration is finalised. The IMU data assists the system to find the rotation around the centre of the coordinate system in each time stamp using the rotation matrix (D. Lee et al., 2011). This takes into account movement, and its rotation around the centre of the coordinate system.

The initial global drone position estimation has been done according to a known global marker value (G), detected initially by the system. The overview of this procedure has been illustrated in Figure 4.2. The known global coordinate value of the marker is denoted by (x_G, y_G, z_G) . $d_{\Delta t}$ represents movement distance interval $d_{\Delta t}$ according to IMU data where $(x_{D_{t_0}}, y_{D_{t_0}}, z_{D_{t_0}})$ is the drone global coordinate value according to the marker distance. In state t_0 , $(x_{D_{t_1}}, y_{D_{t_1}}, z_{D_{t_1}})$ is the drone global coordinate value according to movement distance to state t_1 . In Figure 4.2, D indicates distance measured by triangle similarity (Nazem et al., 2019)

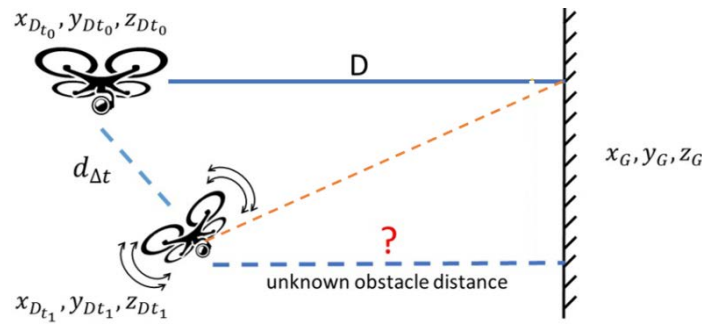


Figure 4.2 Unknown obstacle estimation by IMU and capturing device

4.4 System Implementation

In a navigation application, the IMU sampling provides raw angular velocity from the gyroscopes, acceleration from the accelerometers, and heading processed by roll and pitch from the accelerometers and raw data from magnetometer. The KF is responsible for filtering the information in order to gain useful information. The KF performance and the accuracy of the results severely depend on high speed and constant sensor sampling rate data. The prototype proposed by this study contains the IMU connected to a central processor unit through a micro controller. The central processing unit is responsible for making decisions based on the filtered and processed IMU data, and to send commands to control unit to manipulate drone movement in order to avoid obstacles in INS. Implementation of the initial prototype proposed by this research has two approaches which are IMU handshakes with Raspberry Pi (RPi) through Arduino and IMU handshakes with RPi without any further device using General Purpose Input/output (GPIO) pins. For the application of such approaches, the IMU must first be synchronised with the various sampling sensors.

4.4.1 System Synchronisation

The IMU has three different sensors with different sampling rates. The different sampling frequencies need to be combined through synchronisation. To sync two devices with different frequencies, the data from the higher frequency device must be collected in a specific time interval. The rate of sampling of the higher frequency device to the lower frequency device defines this time interval.

The IMU utilised in this research includes a gyroscope and accelerometer. The accelerometer frequency is set to 260 Hz, and the gyroscope is set to 256 Hz. Capturing device frequency is calculated based on timestamps and number of samples. Considering n is the number of samples, $t = \{t_0, t_1, \dots, t_n\}$ is the sampling period and t_0 to t_n is the time interval, then system period or Δ_t is calculated by:

$$\Delta_t = t_n - t_0 \quad (4.25)$$

To calculate the frequency, which is equal to sampling rate, the number of samples need to be divided by the sampling period:

$$\text{Frequency} = \text{sampling rate} = \frac{n}{\Delta_t} \quad (4.26)$$

To sync two devices with different frequency the data from high frequency device must be collected in the sampling interval defined by:

$$\text{sampling time interval} = \frac{\text{high frequency device}}{\text{low frequency device}} \quad (4.27)$$

4.4.2 Accelerometer, Gyroscope and magnetometer synchronisation

As mentioned in this example, sampling time interval can be calculated by accelerometer frequency divided by magnetometer frequency, therefore for magnetometer and accelerometer the sampling time interval is 4. This sampling time interval is calculated based on the accelerometer frequency being the high frequency sensor, and it in turn is used to calculate the optimised sampling time interval between accelerometer and gyroscope. The frequency of gyro in full power mode (3.2 mA) is 1000 Hz for Output Data Rate (ODR), however it normally operates at 256Hz by default.

The sampling time interval between the accelerometer and gyroscope is obtained from dividing the gyroscope frequency by the accelerometer frequency, which is equal to 32. Considering the common sampling interval, these three sensors can be synced for sample collection task.

- Low power accelerometer mode current: 8.4 μ A at 0.98Hz, 19.8 μ A at 31.25Hz
- Magnetometer normal operating current: 280 μ A at 8Hz repetition rate

$$\text{sampling time interval} = \frac{\text{Accelerometer frequency}}{\text{Magnetometer frequency}} = \frac{32}{0.98} = 4 \quad (4.28)$$

- Gyro operating current: 3.2 mA (full power, gyro 1000 Hz ODR)

$$\text{sampling time interval} = \frac{\text{Gyroscope frequency}}{\text{Accelerometer frequency}} = \frac{1000}{32} = 31.25 \quad (4.29)$$

4.4.3 Synchronisation required for communication between IMU device and processing device.

For communication between the IMU and devices such as a RPi or Arduino (also common for light weight drone operations), the following must be considered. As stated before, the prototype attempts the following:

- IMU handshakes with RPi through Arduino
- IMU handshakes with RPi without any further device using GPIO.

In both methods the connection has been applied by either the I2C or SPI protocol with consistent rate (frequency). For instance, this project in prototype implementation used the I2C standard for communication with the processor unit (Arduino or RPi). The I2C time interval is 25 microseconds for synchronisation.

- 400kHz Fast Mode I2C for communicating with all registers
- 1MHz SPI serial interface for communicating with all registers
- 20MHz SPI serial interface for reading sensor and interrupt registers
- I2C time interval is 25 microseconds

The communication between two devices in an embedded system are based on a set of defined protocols for sending and receiving data (SPI and I2C). SPI uses 4 signals:

- Master Out, Slave In (MOSI) - which is the data going from the master to the slave;

- Master In, Slave Out (MISO) - which is the data going from the slave to the master;
- Serial Clock (SCK) - when this toggles both the master and the slave to sample the next bit of information;
- Slave Select (SS) - this tells a particular slave to go active.

I2C uses 2 signals named SDA and SCL.

- SDA is the data signal for the master and slave to send and receive send and receive data;
- SCL is the clock signal to synchronise data communication.

This research uses the I2C for communication with the processor unit (Arduino or RPi) and IMU. In this case, the master is the embedded controller and the slave is the IMU. The raw data collected by the IMU is sent to the KF. The obtained results sync with the capturing device data. The I2C utilised by this research uses interrupt instead of polling.

4.4.4 First approach – Using RPi only

In the first approach, the devices used are an IMU MPU 9250, a RPi, and a capturing device such as night vision camera. The IMU communicates through an I2C standard (VCC, GND, SDA, SCL) connection to the RPi via its GPIO. The capturing device is connected to the RPi through a FPC or FFC connector. The RPi, after processing data of these two devices and making a final decision, can then send commands to the drone ESC (electric speed controller) motor controller through GPIO PWM (pulse width modulation).

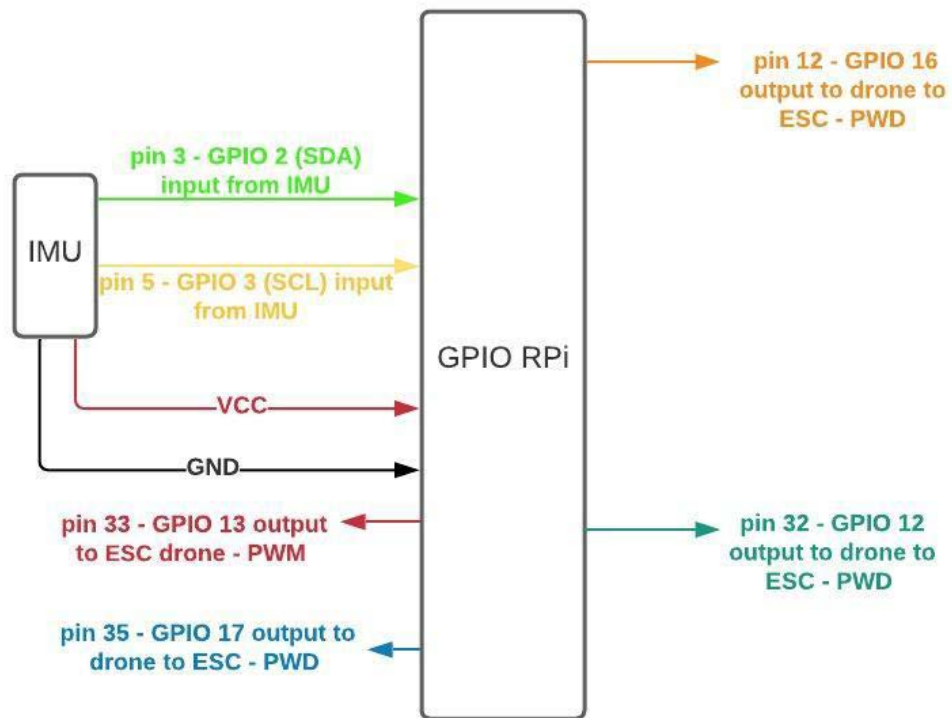


Figure 4.3 First approach prototype

The implementation of this approach proved that the RPi processor cannot handle the input data from the device in terms of processing (capturing device), filtering (IMU data), and communicating the results of final decisions to the motor controller in a time efficient manner. Therefore, in the next approach this project added an Arduino as a micro controller to be independently responsible for the IMU data, and to send the filtered and ready to use information to the RPi in order to reduce the processing load of the RPi and to support it. Table 4.1 shows the navigation system timing by steps.

Steps	Timing (seconds)
I2C Initialization	65miliseconds
IMU initialization and calibration	1.6 second
IMU data generation	0.5 second
IMU data integration and roll and pitch calculation	1958 \pm 0.04microseconds

Table 4.1 Navigation system timing by steps

4.4.5 Second approach – Using Arduino and RPi

The second approach incorporated an IMU MPU 9250, Arduino MiniPRO (328 5v 16Mhz), MiniPR, and RPi equipped with a night vision camera connected to the motor controller. The IMU MPU 9250 is connected to the Arduino through either the I2C or SPI protocol, the I2C is used by this research. The Arduino is attached to the RPi through USB and supplied by an external battery. In the initial prototype, the reason behind using an Arduino as a microcontroller was for collecting, saving, processing and integrating IMU data. The RPi is involved in finding a marker location by true matching key points between two consecutive frames captured by the night vision camera to find depth in two consecutive time intervals. Additionally, the RPi is responsible for making decisions and sending commands through GPIO PWM pins to the ESC to manipulate the drone. These commands are made from the final RPi decision making considering the data provided by the IMU, and information extracted from the frames captured by the camera. The integrated data by the Arduino was sent through USB0 with a baud rate of 4800 to the RPi. This means that the serial port is capable of transferring a maximum of 4800 bits per second. Figures 4.2 and 4.3 illustrate the initial and final prototype. Using the RPi GPIO is an alternative method for connecting the IMU to RPi, and removes the Arduino as an extra power consumer. However, the Arduino is needed for parallel processing. This second approach showed better results compared to the first approach in regards to timing and implementation. Table 4.1 indicates timing for both approaches. Second approach is proposed because of its low power consumption whereas timing is the same as the first approach.

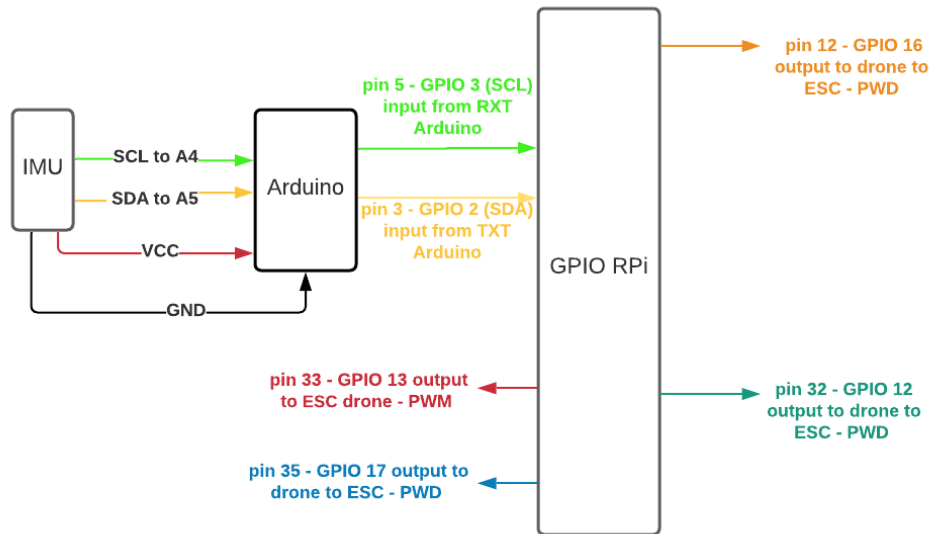


Figure 4.4 Second approach prototype

4.5 Chapter Summary

This research designed a prototype for drone self-navigation in GNSS-denied underground mines. This prototype used a small and a very basic IMU. To address gyro drift, roll and pitch were obtained using the accelerometer data, and yaw was extracted by the integrated roll, pitch and magnetometer data. The system was designed for education and training purposes and still contained noise, which was unpredictable. The IMU provided the information to gain movement distance in each time interval. The second prototype experimental results proved that the KF is essential in filtering out noise and helping to reduce propagation of errors and ensures that it can be processed by the system. As mentioned before the drift and noise in this system are stochastic (not predictable) accumulative and not deterministic (predictable). Designing Kalman for this system allows opportunity to predict the next state. The limitation of using a KF for all aspects is the lack of a powerful processing system for such applications, as the RPi needs to process the IMU data and capturing device data in parallel. In case of using an Arduino to support the Raspberry pi in the processing required, the system encountered power consumption issues that requires extra power to the system, which leads to increase the weight of the whole drone system.

5 EXPERIMENTAL RESULTS

5.1 Introduction

The full process for autonomous positioning for drone in in underground mining consists of two modules. The first module is responsible for detecting manmade markers utilising an image capturing device. This data is processed to obtain the distance between drone and the marker which global coordinates are known. Then, the second module is responsible for processing the data collected from the IMU device to obtain the drone orientation and position while flying. This includes the IMU initialisation, calibration and data processing. This research focuses on the results of the second module. Figure 5.1 depicts an overview of the combined modules. The blue blocks indicate the parts attributed to the second module (this research), while the remaining blocks denote the steps to be implemented in another study. Nazemi et al. (2021) explained in detail the implementation of first module (Nazemi et al., 2021).

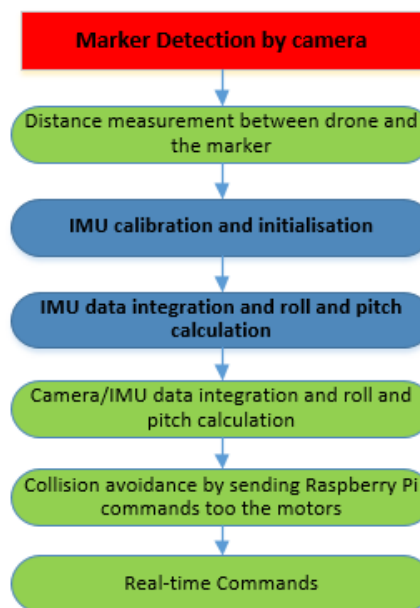


Figure 5.1 Drone autonomous positioning system overview

This chapter presents the experimental results of this study from basic to advance movement. Six different scenarios are defined to observe the behaviour of the IMU sensors before and after using the KF. This study was carried out in a laboratory

environment due to the lack of access to measurement sensors output data in a mining environment, and the ability to control the motion and environment. Roll, pitch and yaw were calculated as the reliable parameters for the IMU behaviour recognition. These results aid the research in troubleshooting the sensors and processing in terms of increasing accuracy in calibration, synchronisation and the filtering method. At the end of the implementation of these six scenarios, sample datasets for IMU were obtained according to the following scenarios:

- Activity: pedometer
- Environment: freefall, orientation
- Gestures: tap, double tap
- Tasks: picking up an object

5.2 IMU specifications

The test setup was designed to allow the application of specific algorithms and viewing the results of different scenarios for better understanding of position and orientation determination utilising IMU MPU 9250. This section studies different situations and the IMU behaviour, as shown in the following sections. The following are the IMU manufactural characteristics considered in this section (TDK, 2021):

- Accelerometer Range = +/- 6g
- Gyroscope Range = +/- 2000 degrees/second
- Magnetometer Range = +/- 200uT

This data is from real time measurements.

5.3 Initialisation and Calibration

The IMU sensors need to be calibrated regardless of any filter implementation. Initialisation must take place before utilisation. As discussed in section 3.4, prior to starting the measurements, the IMU initialisation (warm up) is part of the normal start-up process. Depending on the ambient temperature when the IMU was calibrated, the 'warm up' period can be a few seconds to several minutes. For the IMU used in this research, it takes roughly 8 second to initialise. Accelerometer bias is represented by

(a_x, a_y, a_z) and obtained (-86.91, -37.84, -11.17) [m/s^2]. Gyro bias is represent by (g_x, g_y, g_z) obtained these values (1.50, -0.50, 0.70) [deg/s] (TDK, 2021).

5.4 IMU filtering results overview

This section uses the obtained experimental data depicted in the all scenarios, the values from the applied KF to the system, and compares the raw data against the filtered results. The raw values (unfiltered) are shown coloured red and the filtered values are shown coloured blue in all Figures. The objective of this section focuses on the comparison of the raw and filtered data in relation to the roll, pitch and yaw measurement.

Section 4.2 in the previous chapter explained the KF implementation used in this research. Roll, pitch and yaw were calculated using equations 3.1, 3.2 and 3.5. As detailed in Figure 4.1, only the accelerometer data are used in zero state for these equations. For states greater than zero, the gyroscope is used in order to benefit from its sensitivity to changes. All equations in chapter 4 are applied to the gyro components instead of the accelerometer components. This means where vertical movement (along y-axis) takes place for state zero, a_y is changed and for other states g_y is changed. This is because based on equations 3.1, 3.2 and 3.5, when a_y is changed, roll also varies. When horizontal movement happens a_x changes in the equations in state zero, and for other states g_x is changed, hence the value for pitch is also affected and movement in depth means movement along z-axis.

Within previous Figures, in terms of roll, pitch and yaw, a ramp is present at the beginning as a result of using the accelerometer in state zero. The purpose of all scenarios are observation of IMU performance and ability in the presence of sudden acceleration and deceleration of the system. All the Figures illustrate that the KF at the end of the timing period makes the presented curves more stable and smoother. The reason behind this behaviour is that based on the conditions applied in Figure 4.1, it uses the state at interval $t - 1$ to t and the value at state t based on the predicted value.

Due to sudden changes in the system, drift increases exponentially which causes a delay in the KF performance. This leads to a lag which can be observed.

As observed in previous Figures, yaw is firmly dependant on roll or/and pitch. If in a specific scenario, when acc_x or movement in x is observed, the change in roll becomes noisy, which consequently leads to a noisy yaw. If the acc_y or movement in y occurs, pitch becomes noisy, which in turn also causes noisy yaw values. This is because, as previously described, yaw is a function of roll and pitch. In all figures, negative roll, pitch and yaw values indicate clockwise rotation and positive values denote anticlockwise rotation. Generally, if changes in the horizontal are more than changes in the vertical, then the roll will be noisier. If changes in the vertical are more than the changes in horizontal, then the pitch will be noisier.

5.4.1 Dropping scenario

In this scenario, the data was collected when the IMU was dropped from a table. A cushion was used to prevent IMU damage. The purpose of this scenario is to test the IMU abilities in the presence of a sudden acceleration and deceleration of the system. Figure 5.2 shows the comparison of the unfiltered (red) versus the filtered (blue) data for the roll values. The blue line represents the filtered data as described by the KF in chapter 4.

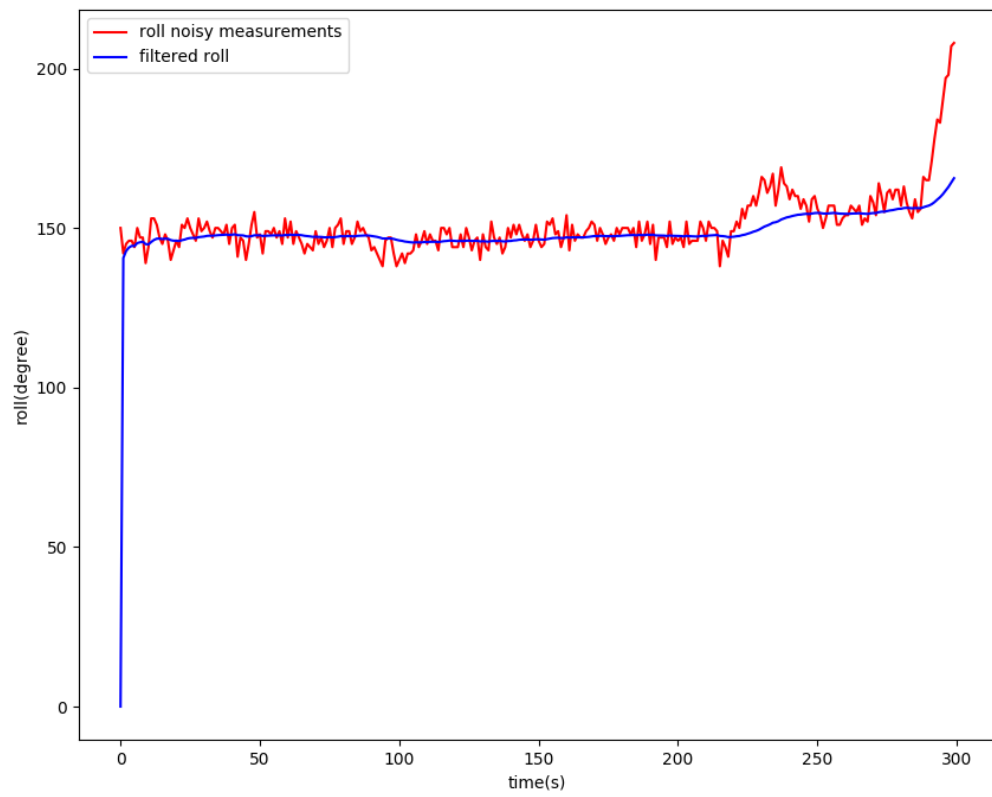


Figure 5.2 The raw measurements for the roll data (red) plotted against the data processed by the KF (blue) for the dropped scenario.

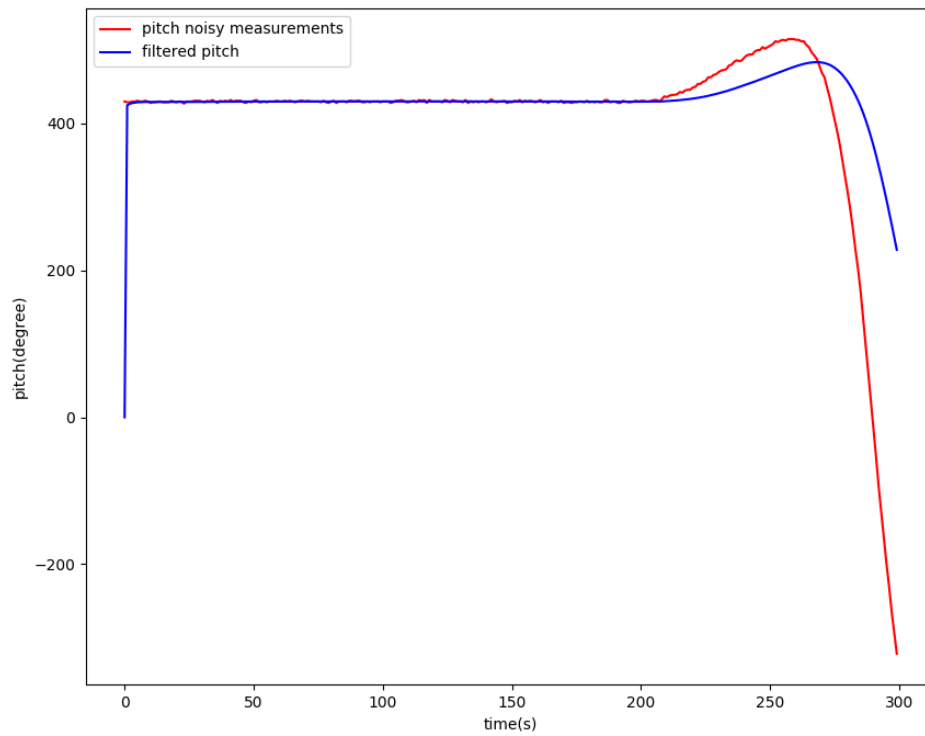


Figure 5.3 The raw measurements for the pitch data (red) plotted against the data processed by the KF (blue) for the dropped scenario.

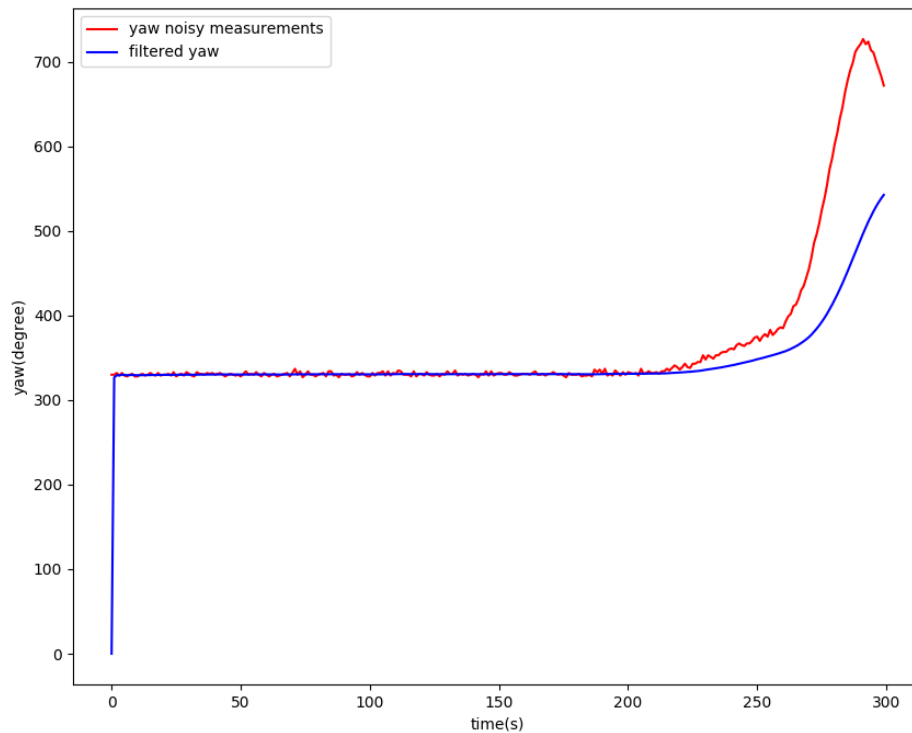


Figure 5.4 The raw measurements for the yaw data (red) plotted against the data processed by the KF (blue) for the dropped scenario

Figure 5.2 shows the roll measurement in the dropping situation. The raw roll values are noisier than pitch and yaw, because in this scenario acceleration in y is variable. Pitch does not have a direct relationship with the gyro components in state zero, and it can be calculated using just the accelerometer, thus this is drift free as observed by the red and blue lines being plotted approximately the same with respect to each other, as shown in Figure 5.3.

Figure 5.4 shows the yaw measurement in the dropping situation. Yaw firmly depends on roll and/or pitch. In this specific scenario acceleration in x is changed so the roll values are noisy. This then will also lead to a noisy yaw. If the acceleration in y changed causing the pitch to be noisy, this will in turn cause a noisy yaw. In the dropping scenario there are three states as follows:

- Push state at $t = 0$
- Dropping state at $0 < t < t - 1$
- Impact state at t

In other words due to large changes in y movement at the impact state (occurring towards the end of the Figures 5.2, 5.3 and 5.4) drift away from the true value increases exponentially which causes a delay in the KF performance and a lag can be observed at the end of the Figures 5.2, 5.3 and 5.4 as the KF cannot trace and address the drift quick enough.

5.4.2 Double tap Scenario

In this scenario the experiment collected data when the IMU is held in the left hand and tapped twice with the right index finger. Figure 5.5, 5.6 and 5.7 shows the comparison of the unfiltered (red) versus the filtered (blue) data. The red line illustrates that the roll measurement using the gyro has noticeable noise in Figure 5.5. The blue line represents the filtered data using the described KF.

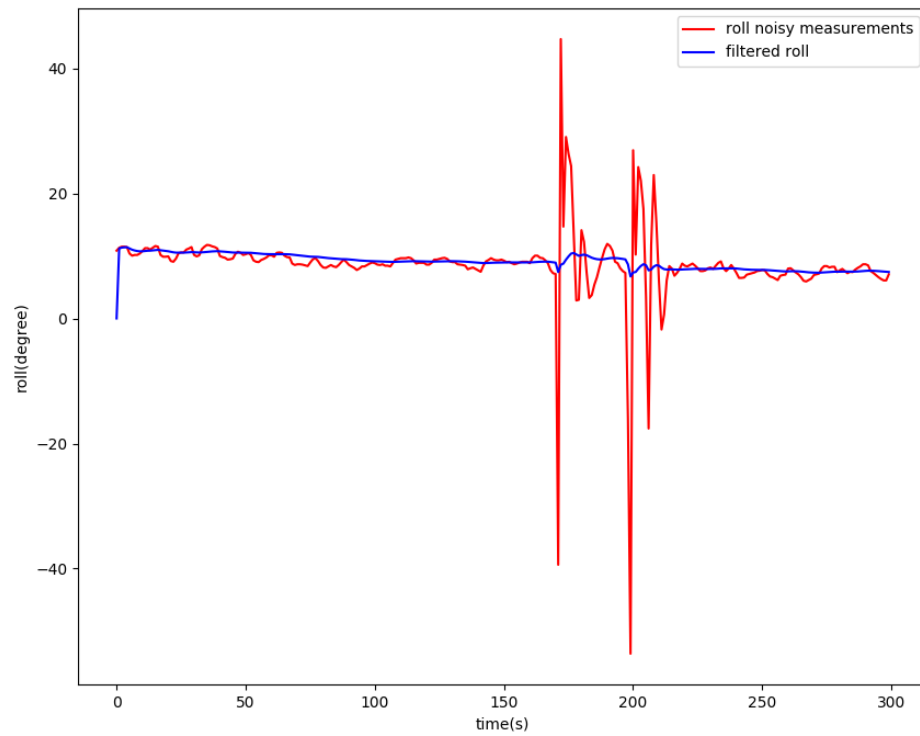


Figure 5.5 The raw measurements for the roll data (red) plotted against the data processed by the KF (blue) for the double tap scenario

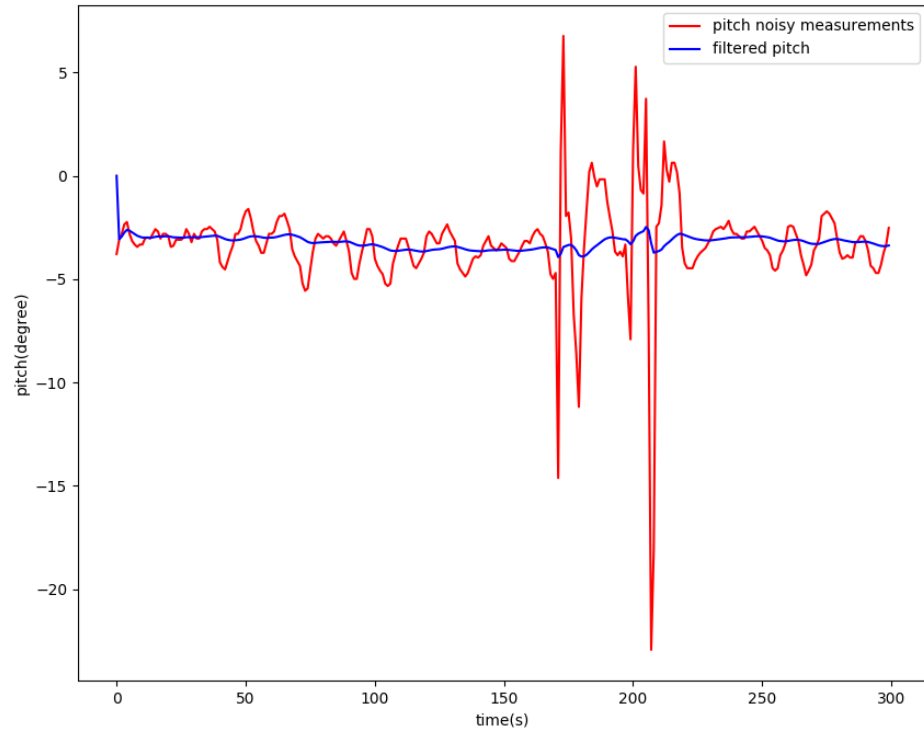


Figure 5.6 The raw measurements for the pitch data (red) plotted against the data processed by the KF (blue) for the double tap scenario

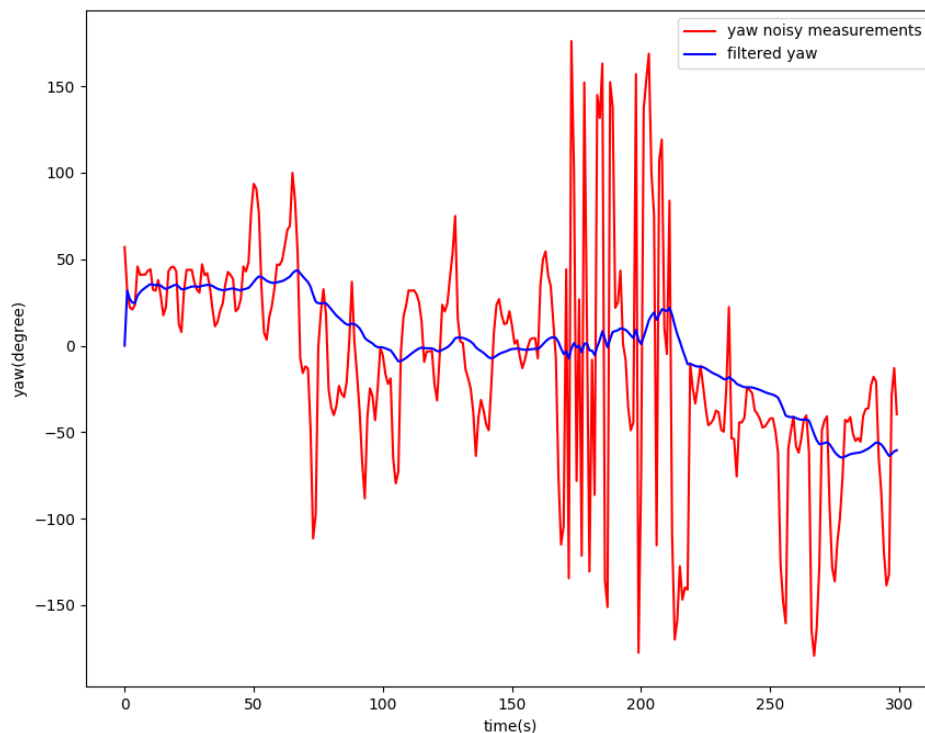


Figure 5.7 The raw measurements for the yaw data (red) plotted against the data processed by the KF (blue) for the double tap scenario

Figures 5.5 and 5.6 show the roll and pitch measurement in double tap situation. In this scenario the roll and pitch seem to have similar signals because both are affected by the position in the x and y direction being changed. This also leads to a noisy yaw value (seen in figure 5.7), as yaw is a function of roll and pitch. The double tap can be seen clearly in the roll and pitch raw data in figure 5.5 and 5.6 as the two spikes in the data. Also shown in Figures 5.5, 5.6 and 5.7 the KF appears to be well suited to filtering out the large spikes and generating the near constant response that is expected since there was little orientation change in the system during the data capture. It can also be seen that it improves the filtered yaw values presented in figure 5.7 compared to the raw values.

5.4.3 Walking scenario

In this scenario the collected experiment data is from when the IMU Sensor is in the left front pocket of a person walking approximately 25 meters in a straight line. Physical movement happens in both the vertical and horizontal axis, as seen in Figures 5.8, 5.9 and 5.10 for this specific scenario, both roll and pitch have noticeable noise, and consequently yaw (being a function of roll and pitch combined) is also noticeably affected by the noise from both roll and pitch.

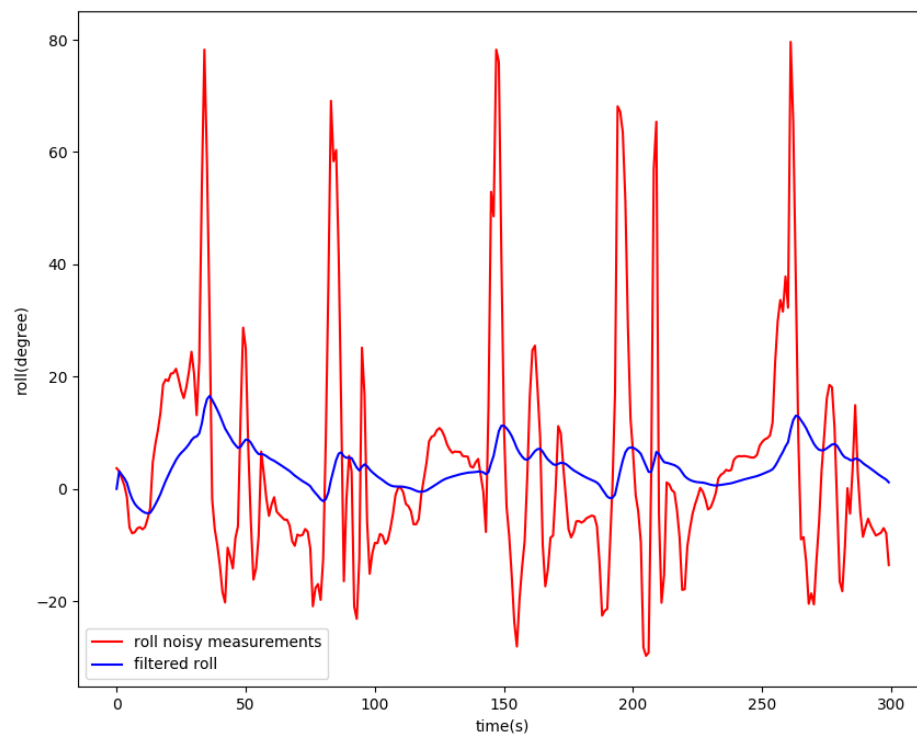


Figure 5.8 The raw measurements for the roll data (red) plotted against the data processed by the KF (blue) for the walking scenario

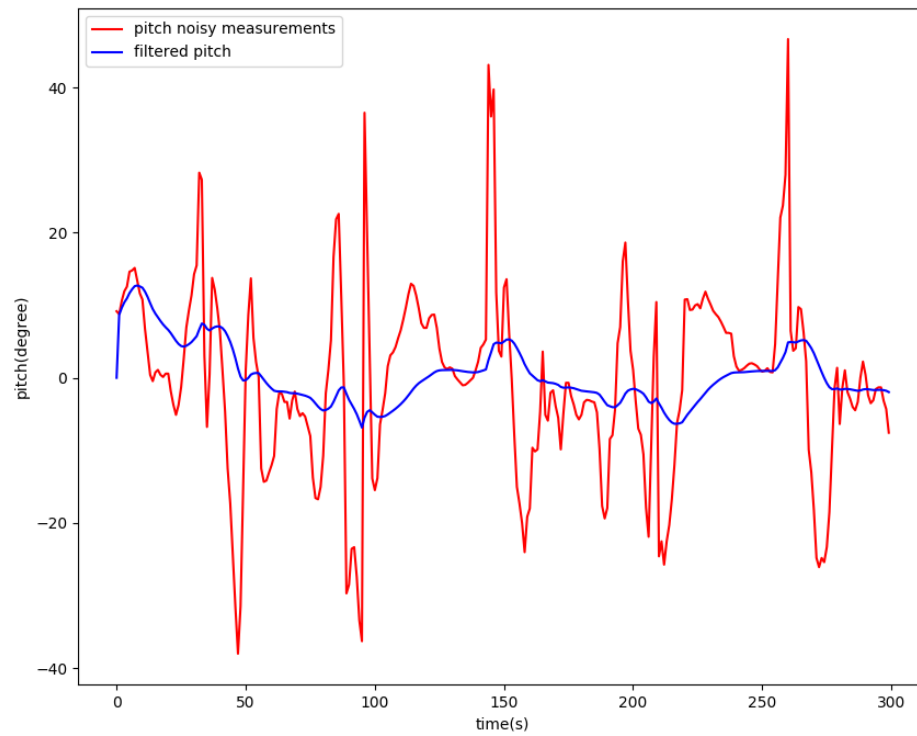


Figure 5.9 The raw measurements for the pitch data (red) plotted against the data processed by the KF (blue) for the walking scenario

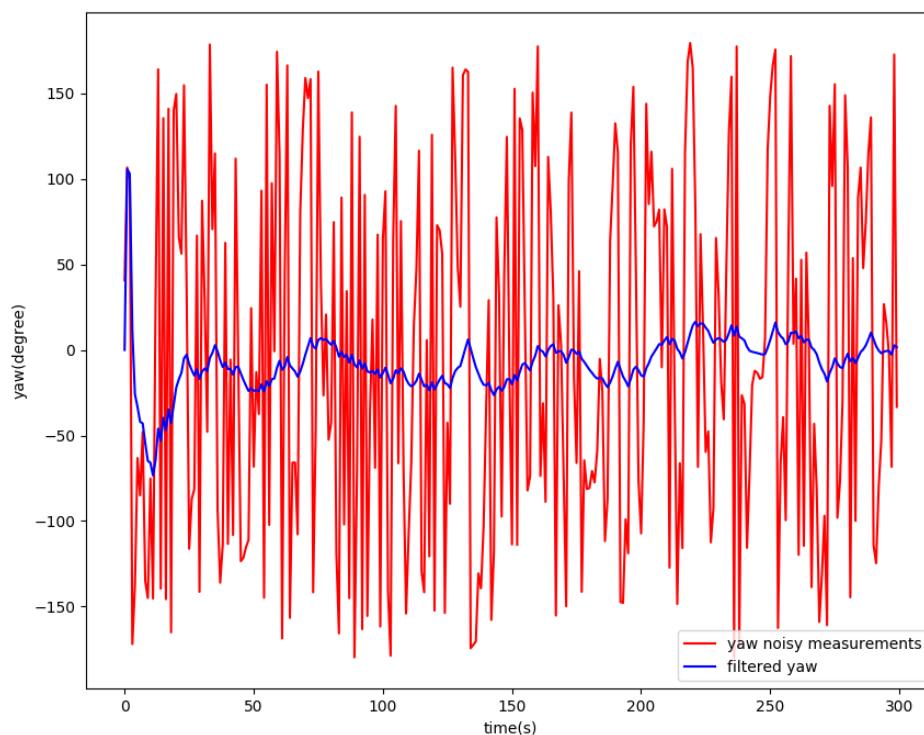


Figure 5.10 The raw measurements for the yaw data (red) plotted against the data processed by the KF (blue) for the walking scenario

Given the nature of walking in a straight line, the orientation should be relatively stable, except for the peaks and dips corresponding to the walking gait of a person, which is periodic in nature. As can be seen in Figure 5.8 and 5.9, the raw data has significant noise due to this (red line). By applying the KF, these large deviations are filtered out leaving a more consistent orientation profile (blue line). Examining the yaw values in figure 5.10, the raw values are noisy to the point of being unable to determine a consistent heading, whereas the filter values in blue show a more constant heading, which is expected from walking in a straight line. The yaw is now more consistent to within a range of 15 degrees, and the accumulated affect from the roll and pitch has been significantly reduced.

In the walking scenario there are three states as follows:

- Start walking state at $t = 0$
- walking state at $0 < t < t - 1$
- stop walking state at t

5.4.4 Horizontal nudge of IMU

In this scenario the experiment collected data when a horizontal nudge to the IMU has occurred.

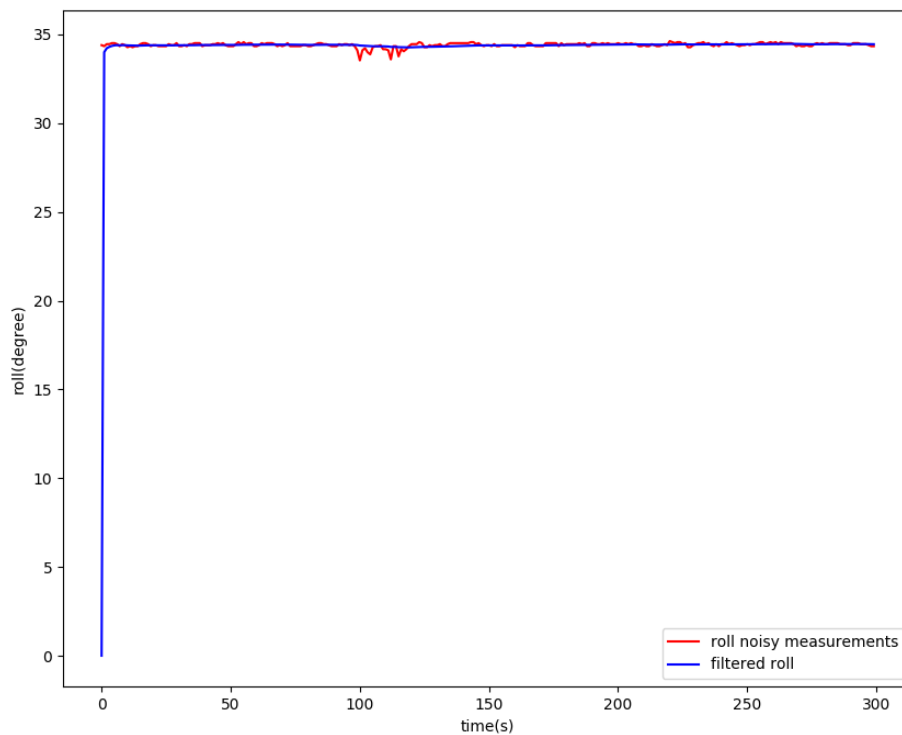


Figure 5.11 The raw measurements for the roll data (red) plotted against the data processed by the KF (blue) for the horizontal nudge scenario

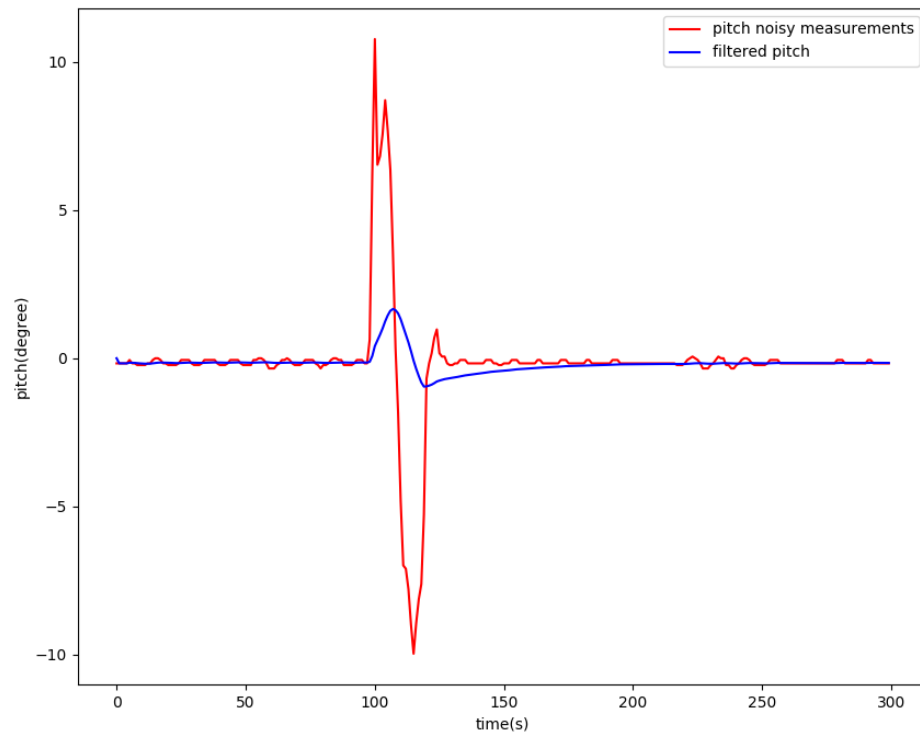


Figure 5.12 The raw measurements for the pitch data (red) plotted against the data processed by the KF (blue) for the horizontal nudge scenario

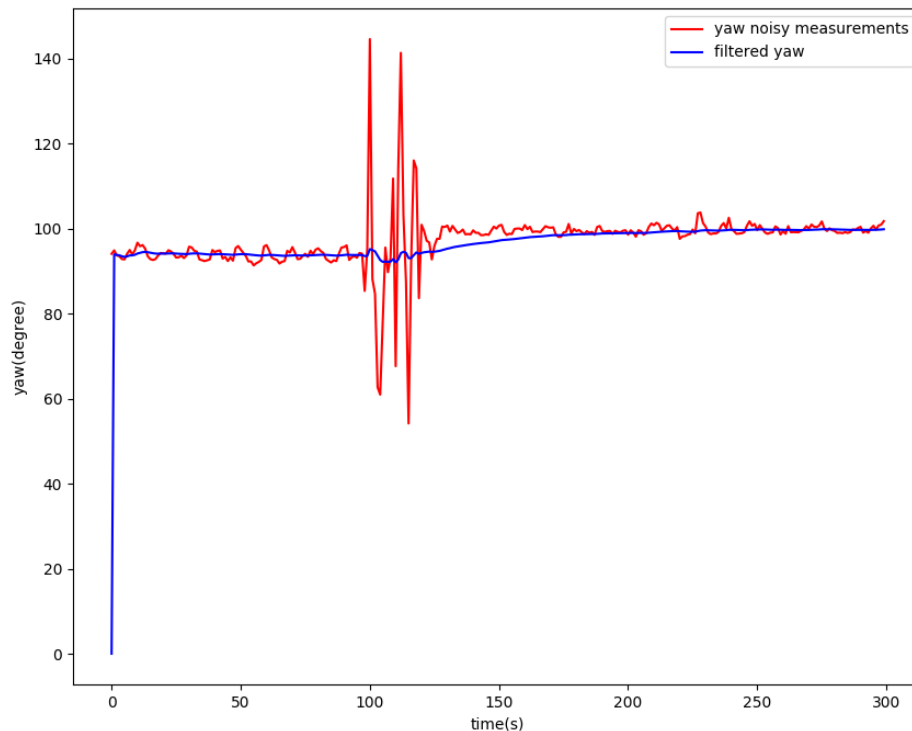


Figure 5.13 The raw measurements for the yaw data (red) plotted against the data processed by the KF (blue) for the horizontal nudge scenario

Figures 5.11 and 5.12 show the roll and pitch measurement in horizontal nudge situation. The change in the x direction causes the pitch to be noisy as the nudge was in this direction and not the y direction, hence why there is very little noise evident in the roll data. The noise in pitch also leads to noisy yaw values. In the case of the applied horizontal nudge, the effect has been completely filtered out in all except the pitch data (Figure 4.12), which is the desired outcome.

From the state zero until the nudge impact is applied, the drift can be ignored as slight. Then one big spike in pitch can be observed at the impact moment. Besides filtering out the noise, and the effect of the nudge in the roll and yaw, there does seem to be a bit of a lag in the filtering of the pitch and yaw. This is because of the lag in the filter to adapt to the rapid change caused by the nudge.

5.4.5 Fast pickup IMU

In this scenario, the experiment was conducted to collect data when the IMU was pick up from a table quickly. Due to large changes in y movement at the ending state (occurring towards the end of the figure) drift away from the true value is increased exponentially which causes a delay in the KF performance and a lag can be observed at the end of the figures as the KF cannot trace and address the drift quick enough. As observed in this scenario, there is an inconsistency in roll, pitch and yaw towards the end of Figure 5.14, 5.15, and 5.16. The reason behind this is due to the acceleration from the fast movement. In this case, the only one that appears to be highly noisy is the roll data, because the IMU was only moved vertically. Figure 5.14 shows the comparison of the unfiltered (red) versus the filtered (blue) data.

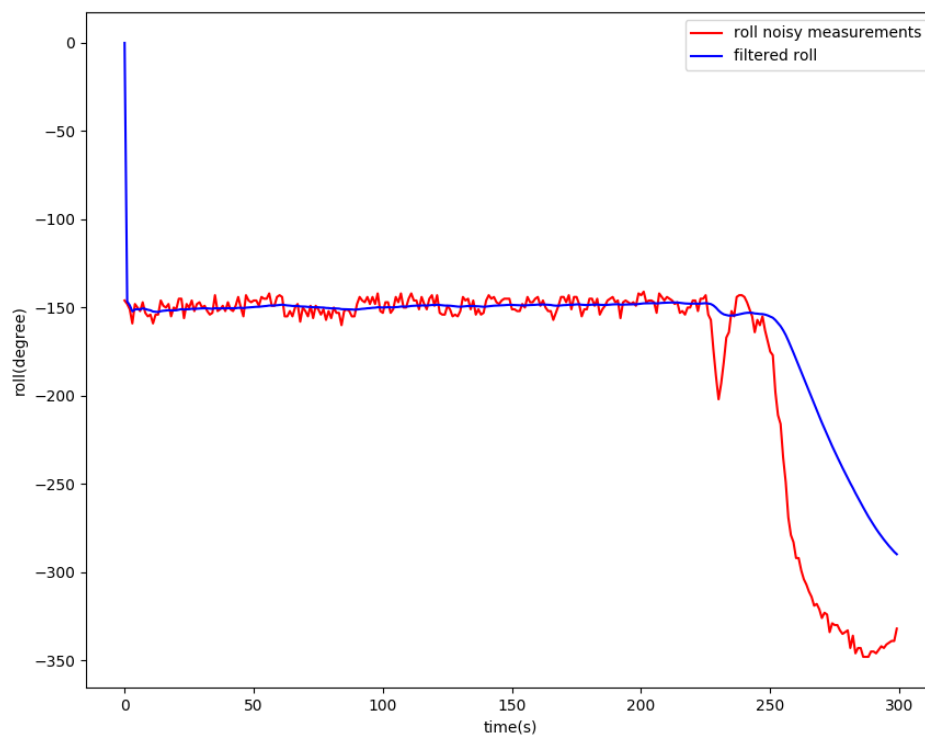


Figure 5.14 The raw measurements for the roll data (red) plotted against the data processed by the KF (blue) for the fast pickup scenario

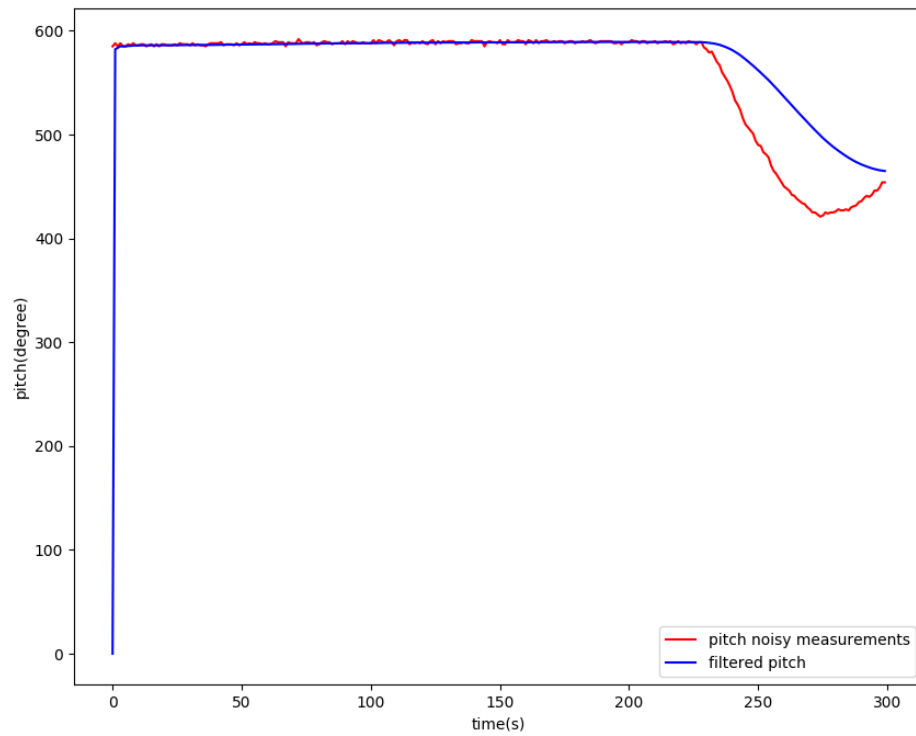


Figure 5.15 The raw measurements for the pitch data (red) plotted against the data processed by the KF (blue) for the fast pickup scenario

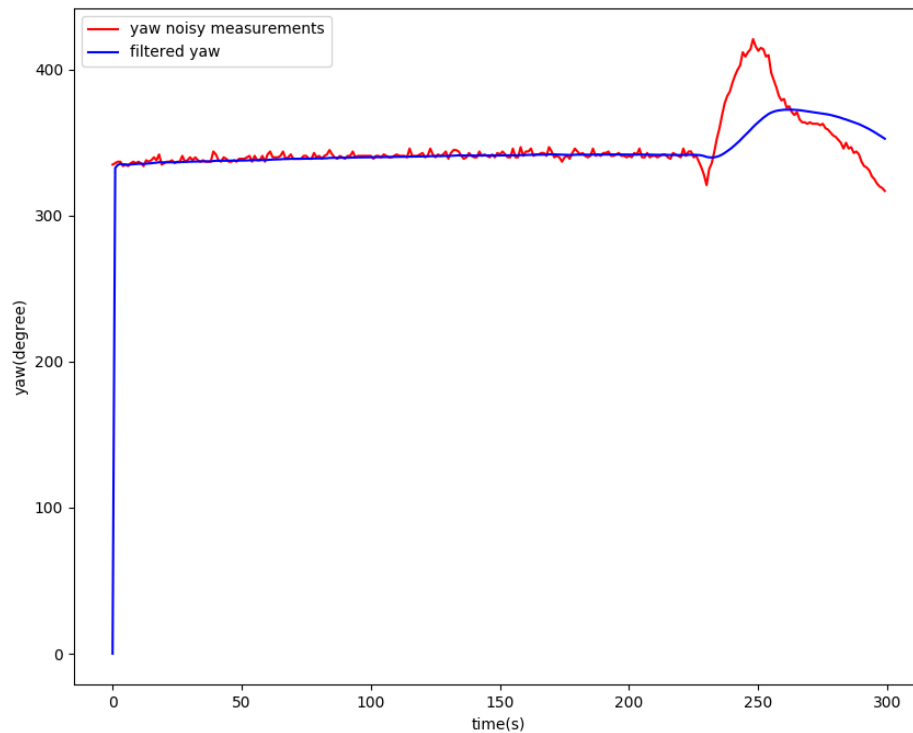


Figure 5.16 The raw measurements for the yaw data (red) plotted against the data processed by the KF (blue) for the fast pickup scenario

5.4.6 Slow pickup of IMU

In this scenario the experiment collected data when the IMU slowly pick up from table (similar to the scenario in section 5.4.5). Similar to the previous scenario, the roll data exhibits the most noticeable noise. As with the fast pickup in section 5.4.5, the IMU was only moved vertically which causes this response. In this scenario, the rapid acceleration did not occur, which leads to a different result compared to the fast pickup. Figure 5.17 shows the comparison of the unfiltered (red) versus the filtered (blue) data. The red line illustrates that the roll measurement using gyro has noticeable noise, while the blue line represents the filtered data by described KF in chapter 4, which has the noise filtered from the results. At state t or end of the scenario shows that Kalman can address the drift at state $t-1$.

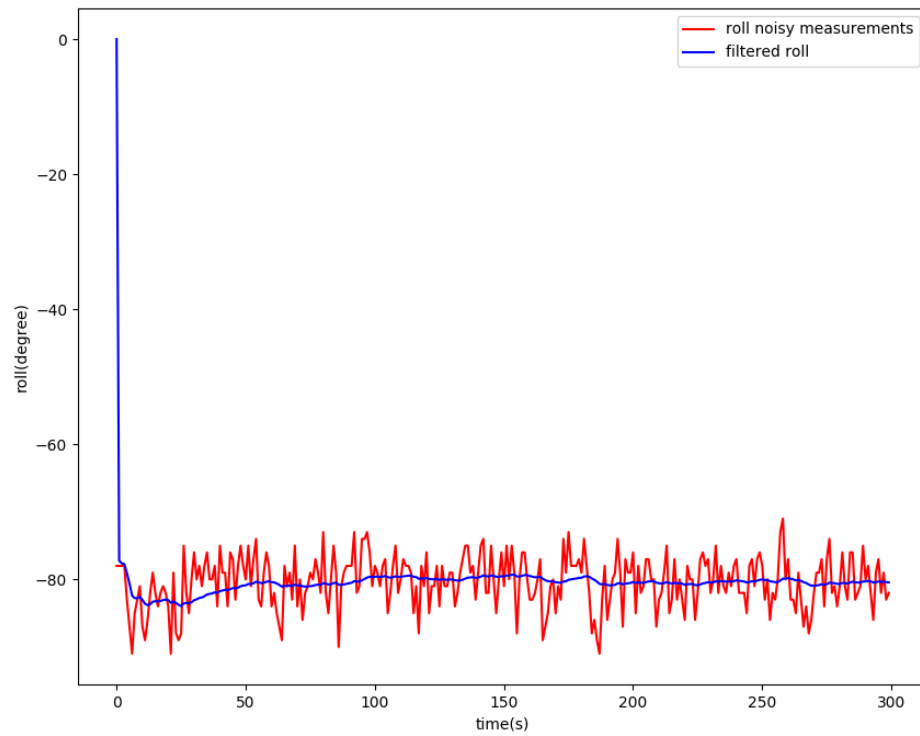


Figure 5.17 The raw measurements for the roll data (red) plotted against the data processed by the KF (blue) for the slow pickup scenario

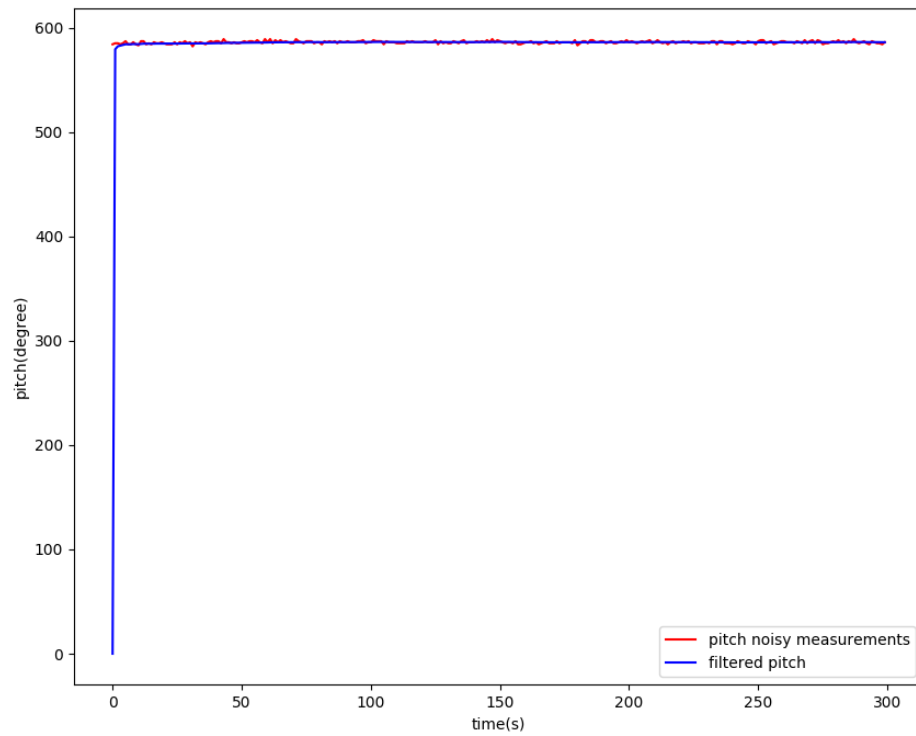


Figure 5.18 The raw measurements for the pitch data (red) plotted against the data processed by the KF (blue) for the slow pickup scenario

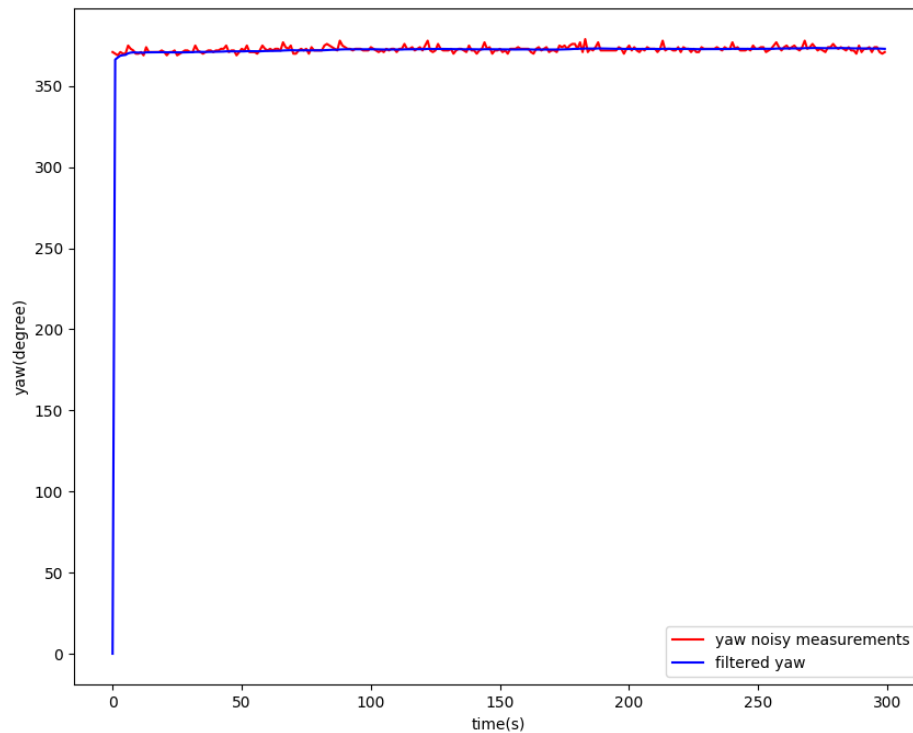


Figure 5.19 The raw measurements for the yaw data (red) plotted against the data processed by the KF (blue) for the slow pickup scenario

Figures 5.14 and 5.17 show the noisy roll measurement in fast pickup and slow pickup of IMU scenario. The roll value is noisier than pitch and yaw, because in this scenario acceleration in y is variable. Figures 5.16 and 5.19 show the yaw measurement in this situation. Yaw firmly depends on roll and/or pitch. If in this specific scenario the acceleration in x is changed, the roll values become noisy, which will then also lead to a noisy yaw. If the acceleration in y changes causing the pitch to be noisy, this will in turn also cause a noisy yaw. For state t or the end of the scenario, a large change did not occur (as with the previous scenario) so the KF can address the drift without any delay or lag. Figure 5.18 (pitch) and figure 5.19 (yaw) show much less noise in the raw data, and the filtered results have a stable value since the orientation did not change significantly during the testing phase.

5.5 Chapter Summary

Various conditions were tested to qualify the IMU behaviour such as shaking, walking, and dropping. This chapter presented six different situations and compared the filtered and unfiltered data. Figures of the measured roll, pitch and yaw data were presented, as well as the data estimated from the application of the KF presented in Chapter 4. All results denote that drift starting after some timestamp, depending on the events occurring in the scenarios, the drift may start immediately or after some timestamp. It was demonstrated that the KF could address these drifts. Within all figures in terms of roll, pitch and yaw, a ramp is present at the start as a result of using the accelerometer to define the zero state. The purpose of all scenarios are observation of the IMU performance, and the ability of the KF to cope in the presence of sudden acceleration and deceleration of the system. These scenarios were designed to obtain reliable ground truth in regard to the IMU performance under different conditions.

Since the purpose of this experiment was observing IMU behaviour in different scenarios effort was made to simulate all unknown situations for IMU as close as accurate laboratory conditions which eventually will lead to IMU behaviour in real flight conditions. In order to achieve this and to tackle complicated scenarios with uncertain conditions the flight scenario was subdivided into plain and more controllable conditions in laboratory environment. Changes in altitude, which is one of the most relevant situations in real flight, was achieved by dropping and picking up the IMU. The results obtained from above said scenarios will help to trouble shoot, calibrate and initialise the IMU.

This research is a part of an ongoing study to address the issues regarding INS in underground mine field. Further developments will be conducted to provide a mine tunnel 3D map using capturing device or night vision camera to aid and assist in the localisation information obtained from this research. Since the data obtain by IMU, even using KF is not sufficient for localisation, the system needs to have another sensor device for data integration. Further development will be conducted to integrate KF data obtain by IMU with another data provided by capturing device.

6 CONCLUSIONS

This research reviewed the autonomous Unmanned Aerial Vehicle (UAV) or drone, in the mapping and surveying in underground mining applications. Specifically, the focus was on the review of the localisation and positioning methods used in such cases. One of the many sensors used for drone self-navigation is Inertial Measurement Unit (IMU). IMU as a positional sensor is used to map required areas in underground mine. This research focuses on low cost IMUs to propose a cost-effective method for localisation and mapping. The improved accuracy of the IMU data provided for localisation is the aim of this study. Mainly focusing on improving raw IMU data through filtering methods to reduce the negative impact of IMU drift in long distances. The collected raw data is corrected by this model to provide more accurate information. This is able to reduce the effect of noise from the environment and the drift of sensors using filters.

This study reviewed localisation and positioning methods including manual, semi-autonomous and autonomous with their advantages and drawbacks. The increase use of drones in inaccessible areas to collect data has led to development of many techniques to overcome the positioning problem and to be able to safely navigate indoors or underground. Sensors play a major role for localization and positioning in UAVs. As discussed in chapter 2, to navigate a drone in an underground mine, three different sensor types are used. These include sensor captures the external environment, inertial sensors to recognise what the drone is doing and the external sensor that give the drone information for localisation and positioning. There are a variety of sensors used within different methods, however IMU sensor is the main focus.

Chapter 3 first examines what an IMU is and the different components that comprise of the system. Detail is then given on each component, focusing on what they measure and how. A comparison of the different methods and IMU types is given based on price and performance. Finally the methods for examining errors in IMUs are highlighted, including compensation methods and current solutions used to mitigate

their effect. Due to IMU data providing information for localisation and positioning it becomes integral and important to all methods.

The four main IMU types used in UAV applications are Silicon MEMS, Quartz MEMS, Fiber Optic Gyroscopes (FOG), and Ring Laser Gyroscopes (RLG). The RLG has the highest accuracy, yet this accuracy comes with financial burden. FOG is a cheaper alternative to RLG. However, it is still expensive and has high power consumption and sensitivity to vibration. Other options are Silicon MEMS and Quartz MEMS IMU. MEMS based IMUs offer acceptable performance while benefiting from low power consumption, small size and price tag. These factors make an IMU a preferred option for navigation system in drone applications. MEMS IMUs are obtained at high sampling rates and can be integrated to obtain position and orientation information. These estimates are accurate on a short time scale, but suffer from integration drift over longer time scales.

The IMU starts collecting data through its sensors, namely, accelerometer, gyroscope and magnetometer, to calculate the roll, pitch, and yaw. This data assists in obtaining the movement distance in each time interval. This information supports the drone in avoiding obstacles. A great challenge regarding utilising IMU is related to sensors' noise and gyroscopic drift. It has the most adverse impact, which exponentially increases over long distances. IMU has an unlimited drift in the velocity, position, and altitude caused by a gyroscope in long distance.

To overcome this issue, inertial sensors are typically combined with additional sensors and models. KF is a suitable candidate for sensor integration. Various methods of filtering may be employed, as discussed in Chapter 3.5. Since the drift and noise in this system are stochastic (not predictable), accumulative, and not deterministic (predictable), this research focused on designing a KF for this specific case.

The reasons behind filtering data in this research is to overcome environmental (compensation) and sensor noise, alongside sensors drifting over time, which affect the IMU data observed. By employing a filter, it allows for the processing and elimination of such adverse effects. Within this research, the filter was used primarily

for the roll and pitch data, not the yaw/magnetometer data. However, based on equation 3.5, the filtered roll and pitch data is still critical for the estimation of the orientation using the magnetometer.

The IMU sensors need to be calibrated regardless of any filter implementation. Initialisation must take place before utilisation. As discussed in Section 3.4, prior to starting the measurements, the IMU initialisation (warm up) is part of the normal start-up process. Depending on the ambient temperature when the IMU was calibrated, the 'warm up' period can be a few seconds to several minutes. For the IMU used in this research, it takes roughly 8 second to initialise. The IMU sampling provides raw angular velocity from the gyroscopes, acceleration from the accelerometers, and heading processed by roll and pitch from the accelerometers and raw data from the magnetometer. The KF is responsible for filtering the information in order to gain useful information. The KF performance and the accuracy of the results severely depend on high speed and constant sensor sampling rate data. Based on its quick response to change, the changes in roll and pitch are calculated by the gyroscope. The gyroscope provides the values of angular velocities along the 3 axes. Gyro sensitivity leads to drift being generated along these rotational axes by accumulation of errors over time. To avoid drift in the gyroscope and to obtain an accurate orientation, a KF is used to integrate two vulnerable sensors, the accelerometer and the gyroscope.

Roll, pitch and yaw were calculated using equations 3.1, 3.2 and 3.5. As detailed in Figure 4.1, only the accelerometer data are used in zero state for these equations. For states greater than zero, the gyroscope is used in order to benefit from its sensitivity to changes. All equations in Chapter 4 are applied to the gyro components instead of the accelerometer components.

Accelerometer and gyroscope are two types of sensors used in motion tracking and control systems. The accelerometer measures linear acceleration (i.e., changes in velocity), while the gyroscope measures angular velocity (i.e., changes in orientation).

In systems that require precise motion tracking, the accelerometer data is used when the state is zero (i.e., when the device is at rest) to determine the initial orientation and

velocity. However, for states greater than zero (i.e., when the device is in motion), the gyroscope is used because of its sensitivity to changes in orientation. This allows the system to track changes in orientation more accurately than using the accelerometer alone, which can be affected by other factors such as gravity.

In summary, the choice of using either the accelerometer or the gyroscope depends on the state of the device, with the accelerometer being used for zero state and the gyroscope being used for non-zero states in order to benefit from its sensitivity to changes in orientation.

In Chapter 5, six different situations examined and compared the filtered and unfiltered data. Various conditions were tested to qualify the IMU behaviour such as shaking, walking, and dropping based on explained the KF implementation used in this research. Roll, pitch and yaw were calculated using equations 3.1, 3.2 and 3.5. As detailed in Figure 4.1, only the accelerometer data are used in zero state for these equations. For states greater than zero, the gyroscope is used in order to benefit from its sensitivity to changes. All equations in chapter 4 are applied to the gyro components instead of the accelerometer components. All results denote that drift starting after some timestamp, depending on the events occurring in the scenarios, the drift may start immediately or after some timestamp. It was demonstrated that the KF could address these drifts. Within all Figures in terms of roll, pitch and yaw, a ramp is present at the start as a result of using the accelerometer to define the zero state. The purpose of all scenarios are observation of the IMU performance, and the ability of the KF to cope in the presence of sudden acceleration and deceleration of the system. These scenarios were designed to obtain reliable ground truth in regard to the IMU performance under different conditions.

Within Figures 5.2-5.7, 5.11, and 5.13-5.15, in terms of roll, pitch and yaw, a ramp is present at the beginning as a result of using the accelerometer in state zero. The purpose of all scenarios are observation of IMU performance and ability in the presence of sudden acceleration and deceleration of the system. All the Figures illustrate that the KF at the end of the timing period makes the presented curves more stable and smoother. The reason behind this behaviour is that based on the conditions

applied in Figure 4.1, it uses the state at interval $t-1$ to damp down the value at state t based on the predicted value. Due to sudden changes in the system, drift increases exponentially which causes a delay in the KF performance. This leads to a lag which can be observed at the end of Figures 5.2-5.7.

As observed in Figures 5.4, 5.7, 5.10, 5.13, 5.16 and 5.19 yaw is firmly dependant on roll or/and pitch. If in a specific scenario, when acc_x or movement in x is observed, the change in roll becomes noisy, which consequently leads to a noisy yaw. If the acc_y or movement in y occurs, pitch becomes noisy, which in turn also causes noisy yaw values. This is because, as previously described, yaw is a function of roll and pitch. Generally, if changes in the horizontal are more than changes in the vertical, then the roll will be noisier. If changes in the vertical are more than the changes in horizontal, then the pitch will be noisier.

The prototype proposed by this study contains the IMU connected to a central processor unit through a micro controller. The central processing unit is responsible for making decisions based on the filtered and processed IMU data, and to send commands to control unit to manipulate drone movement in order to avoid obstacles in INS. Implementation of the initial prototype proposed by this research has two approaches which are IMU handshakes with Raspberry Pi (RPi) through Arduino and IMU handshakes with RPi without any further device using General Purpose Input/output (GPIO) pins. For the application of such approaches, the IMU must first be synchronised with the various sampling sensors.

This research also implements a prototype using Raspberry Pi to process data collected by an IMU and filtered by a KF. The prototype suggest using capturing device such as night vision camera to continuously capture frames of travel area to measure depth or distance to the obstacle. In addition synchronisation between IMU and capturing device will be required. Conclusively another avenue of research will be open for further development. The main target of future research is integrating of IMU and capturing device data to avoid drone collision.

This research is a part of an ongoing study to address the issues regarding INS in underground mine field. Further developments and future research will be conducted to provide a mine tunnel 3D map using capturing device or night vision camera to aid and assist in the localisation information obtained from this research. Since the data obtain by an IMU, even using KF is not sufficient for localisation, the system needs to have another sensor device for data integration. Further development will be conducted to integrate KF data obtain by IMU with another data provided by capturing device.

7 REFERENCES

- Aguilar, W. G., Rodríguez, G. A., Álvarez, L., Sandoval, S., Quisaguano, F., & Limaico, A. (2017, 2017//). Visual SLAM with a RGB-D Camera on a Quadrotor UAV Using on-Board Processing. Paper presented at the Advances in Computational Intelligence, Cham.
- Ahmad, N., Ghazilla, R. A. B. R., Khairi, N. M., & Kasi, V. (2013). Reviews on Various Inertial Measurement Unit (IMU) Sensor Applications. Paper presented at the SiPS 2013.
- Alami, R., Chatila, R., Fleury, S., Ghallab, M., & Ingrand, F. (1998). An architecture for autonomy. *Int. J. Robot. Res.*, 17(4), 315-337.
- Alatise, M. B., & Hancke, G. P. (2017). Pose Estimation of a Mobile Robot Based on Fusion of IMU Data and Vision Data Using an Extended Kalman Filter. *Sensors (Basel)*, 17(10), 2164. doi:10.3390/s17102164
- Anderson, A. (2013). Mining Safety Law in Australia / Aaron Anderson. Chatswood, N.S.W.: Chatswood, N.S.W. : LexisNexis Australia.
- arcelormitta. (2021). Semi-autonomous drilling. Retrieved from <https://corporate.arcelormittal.com/media/case-studies/semi-autonomous-drilling>
- Autonomy, N. E. (2016). M2. Retrieved from <https://www.nearearth.aero>
- Bailey, T., & Durrant-Whyte, H. (2006). Simultaneous localization and mapping (SLAM): part II. *IEEE Robotics & Automation Magazine*, 13(3), 108-117. doi:10.1109/MRA.2006.1678144
- Bakambu, J. N., & Polotski, V. (2007). Autonomous system for navigation and surveying in underground mines. *J. Field Robotics*, 22(12), 829-847. doi:10.1002/rob.20213
- Bakambu, J. N., Polotski, V., & Cohen, P. (2004). Autonomous system for exploration and navigation in drift networks. 2004 Ieee Intelligent Vehicles Symposium, 212-217.
- Baranek, R., & Solc, F. (2012). Modelling and control of a hexa-copter (pp. 19-23).
- Barua, A., Premchand, M. P., Vishnu, R., Dubey, P. K., Jayachitra, A., Gopinath, A. K., Anitha, S., Keezhoth, R., Madeckal, A. P., Karthikeyan, D., Antony, S., Suresh Babu, J., Manohara Rao, R., Sudar, I., & Padmakumar, E. S. (2018). Integrated Navigation, Guidance and Control System and Validation. *Current science (Bangalore)*, 114(1), 109. doi:10.18520/cs/v114/i01/109-122
- Bianco, W., Gerhart, D., & Nicolson-Crotty, S. (2017). Waypoints for Evaluating Big Science. *Social science quarterly*, 98(4), 1144-1150. doi:10.1111/ssqu.12467
- Bottasso, C., Pizzinelli, P., Riboldi, C. E. D., & Tasca, L. (2014). LiDAR-enabled model predictive control of wind turbines with real-time capabilities. *Renew. Energy*, 71, 442-452. doi:10.1016/j.renene.2014.05.041
- Brossard, M., Barrau, A., & Bonnabel, S. (2020). AI-IMU Dead-Reckoning. *IEEE transactions on intelligent vehicles*, 5(4), 585-595. doi:10.1109/TIV.2020.2980758
- Cox, I. J. (1991). Blanche-an experiment in guidance and navigation of an autonomous robot vehicle. *Robotics and Automation, IEEE Transactions on*, 7(2), 193-204. doi:10.1109/70.75902

- cprime. (2020). <https://archer-soft.com/blog/lidar-vs-radar-pros-and-cons-autonomous-driving>. Retrieved from <https://archer-soft.com/blog/lidar-vs-radar-pros-and-cons-autonomous-driving>
- DATA61. (2020). Advanced 3D Mapping and Localisation. Retrieved from <https://research.csiro.au/robotics/our-work/research-areas/3d-lidar-mapping/>
- Dong, Y. (2013). MEMS Inertial Navigation Systems for Aircraft (pp. 177-219).
- Donovan, J., & Lebaron, A. (2009). A Comparison of Photogrammetry And Laser Scanning For the Purpose of Automated Rock Mass Characterization.
- Fernandez, A. (2013). Getting started with the MSP430 LaunchPad / Adrian Fernandez, Dung Dang (1st edition. ed.).
- Flyability. (2014). Elios. Retrieved from <https://www.flyability.com>
- Gede, G. (2011). Introduction to Kalman Filtering
An Engineer's Perspective.
- Gui, P., Tang, L., & Mukhopadhyay, S. (2015, 15-17 June 2015). MEMS based IMU for tilting measurement: Comparison of complementary and kalman filter based data fusion. Paper presented at the 2015 IEEE 10th Conference on Industrial Electronics and Applications (ICIEA).
- He, R., Zhao, Y., Wu, X., & Hu, Z. (2019). A review of UAV monitoring in mining areas: current status and future perspectives. *International Journal of Coal Science & Technology*, 6(3), 320-333. doi:10.1007/s40789-019-00264-5
- Heber, A. (2013). Australian Mining Prospect Award Winners: Excellence in Mine Safety, OH&S - Enware Australia. Australian Mining.
- Hemanth, K. S., Talasila, V., & Rao, S. (2012). Calibration of 3-axis Magnetometers. *IFAC Proceedings Volumes*, 45(1), 175-178. doi:<https://doi.org/10.3182/20120213-3-IN-4034.00033>
- Higgins, W. T. (1975). A Comparison of Complementary and Kalman Filtering. *IEEE Transactions on Aerospace and Electronic Systems*, AES-11(3), 321-325. doi:10.1109/TAES.1975.308081
- Hoflinger, F., Muller, J., Rui Zhang, L. M., Reindl, W., & Burgard, W. (2013). A Wireless Micro Inertial Measurement Unit (IMU). *Instrumentation and Measurement, IEEE Transactions on*, 62(9), 2583-2595. doi:10.1109/TIM.2013.2255977
- Hovermap. (2019). Emesent. Retrieved from <https://emesent.io/products/hovermap/>
- Huang, Y., Ma, C., Zhang, Q., Ye, J., Wang, F., Zhang, Y., Hunborg, P., Varvares, M. A., Hoft, D. F., Hsueh, E. C., & Peng, G. (2015). CD4+ and CD8+ T cells have opposing roles in breast cancer progression and outcome. *Oncotarget*, 6(19), 17462-17478. doi:10.18632/oncotarget.3958
- Inkonova. (2018). Inkonova, Drones for Underground Mines, and Inspections. Retrieved from <http://inkonova.se/>
- Ismail, N., Nurhakim, A., & Saputra, H. M. (2018, 4-5 Oct. 2018). The Calculation of Gyroscope Sensor Angles Using Several Integral Methods. Paper presented at the 2018 12th International Conference on Telecommunication Systems, Services, and Applications (TSSA).
- Jacky, C. K. C., Jeroen, D. H., & Henk, L. (2018). Tightly-Coupled Joint User Self-Calibration of Accelerometers, Gyroscopes, and Magnetometers. *Drones*, 2(1), 6. doi:10.3390/drones2010006
- Jahromi, B. S. (2019). Ultrasonic Sensors in Self-Driving Cars. Retrieved from <https://medium.com/@BabakShah/ultrasonic-sensors-in-self-driving-cars-d28b63be676f>

- James, S., Verrinder, R. A., Sabatta, D., & Shahdi, A. (2012). Localisation and mapping in GPS-denied environments using RFID tags (pp. 1-4).
- Jinhong, X., Zhi, L., Yang, Y., Dan, L., & Xu, H. (2011). Comparison and analysis of indoor wireless positioning techniques (pp. 293-296).
- Kapusta, S. I. a. R. (2020). LIDAR for Autonomous System Design: Object Classification or Object Detection? Retrieved from <https://www.analog.com/en/analog-dialogue/articles/lidar-for-autonomous-system-design-object-classification-or-object-detection.html>
- Kok, M., Hol, J. D., & Schön, T. B. (2017). Using Inertial Sensors for Position and Orientation Estimation. doi:10.1561/20000000094
- Kraft, M., & White, N. M. (2013). MEMS for automotive and aerospace applications / edited by Michael Kraft and Neil M. White: Cambridge, UK : Woodhead Publishing Limited.
- Larsson, J., Broxvall, M., & Saffiotti, A. A Navigation System for Automated Loaders in Underground Mines (pp. 129-140). Berlin, Heidelberg: Berlin, Heidelberg: Springer Berlin Heidelberg.
- Lee, D., Lee, S., Park, S., & Ko, S. (2011). Test and error parameter estimation for MEMS — based low cost IMU calibration. *International Journal of Precision Engineering and Manufacturing*, 12(4), 597-603. doi:10.1007/s12541-011-0077-9
- Lee, S., Lee, D., Choi, P., & Park, D. (2020). Accuracy–Power Controllable LiDAR Sensor System with 3D Object Recognition for Autonomous Vehicle. *Sensors*, 20(19). doi:10.3390/s20195706
- Li, Y., Scanavino, M., Capello, E., Dabbene, F., Guglieri, G., & Vilaridi, A. (2018). A novel distributed architecture for UAV indoor navigation. *Transportation Research Procedia*, 35, 13-22. doi:10.1016/j.trpro.2018.12.003
- Loewy, R. G. (2003). Aircraft Avionics. In R. A. Meyers (Ed.), *Encyclopedia of Physical Science and Technology (Third Edition)* (pp. 319-336). New York: Academic Press.
- Ludwig, S. A., & Burnham, K. D. (2018). Comparison of Euler Estimate using Extended Kalman Filter, Madgwick and Mahony on Quadcopter Flight Data (pp. 1236-1241): IEEE.
- Madhavan, R., Dissanayake, M. W. M. G., & Durrant-Whyte, H. F. (1998). Autonomous underground navigation of an LHD using a combined ICP-EKF approach (Vol. 4, pp. 3703-3708).
- Makela, H. (2001). Overview of LHD navigation without artificial beacons. *Robotics and Autonomous Systems*, 36(1), 21-35. doi:Doi 10.1016/S0921-8890(01)00115-4
- Marcellino, D. (2018). An Examination of Ultra-Wideband (UWB) For Positioning & Location Tracking. Retrieved from <https://www.airfinder.com/blog/ultra-wideband-positioning-location-tracking#:~:text=UWB%20indoor%20positioning%20systems%20are,it%20uses%20to%20transmit%20messages>.
- MathWorks. (2020). Calibrate accelerometer located inside MPU-9250 sensor. Retrieved from <https://au.mathworks.com/help/supportpkg/beagleboneblue/ref/calibrateaccel.html#:~:text=During%20calibration%2C%20ensure%20that%20the%20hardware%20is%20stable.&text=Hold%20the%20hardware%20stable%20and,pressing%20upwards%20and%20press%20ENTER>.

- McNab, K. (2012). Autonomous and remote operation technologies - Harnessing the societal benefits for Australia. *AusIMM Bulletin*, 1(2).
- Mine, G. o. W. A.-D. o. (2021). Minerals safety legislation. Retrieved from <http://www.dmp.wa.gov.au/Safety/Minerals-safety-legislation-8321.aspx>
- Moridi, M., Kawamura, Y., Sharifzadeh, M., Chanda, E., Wagner, M., Jang, H. D., & Okawa, H. (2014). Development of underground mine monitoring and communication system integrated ZigBee and GIS.
- Mostafa, M., Zahran, S., Moussa, A., El-Sheimy, N., & Sesay, A. (2018). Radar and Visual Odometry Integrated System Aided Navigation for UAVS in GNSS Denied Environment. *Sensors (Basel)*, 18(9), 2776. doi:10.3390/s18092776
- Murphy, C. (2020). Choosing the Most Suitable MEMS Accelerometer for Your Application. Retrieved from <https://www.analog.com/en/analog-dialogue/articles/choosing-the-most-suitable-mems-accelerometer-for-your-application-part-1.html>
- Nazemi, A., Moghaddam, F., Tavakolian, N., & Afshar, S. Z. (2021). The Prototype for Drone Self-Navigation Utilizing in Underground Mine. *Recent Advances in Computer Science and Communications*, 14(6), 1771-1783. doi:<http://dx.doi.org/10.2174/2666255813666191120120724>
- Noureldin, A. (2013). *Fundamentals of Inertial Navigation, Satellite-based Positioning and their Integration / by Aboelmagd Noureldin, Tashfeen B. Karamat, Jacques Georgy*. Berlin, Heidelberg: Berlin, Heidelberg : Springer Berlin Heidelberg : Imprint: Springer.
- Nurhakim, A., Effendi, M. R., Saputra, H. M., Mardiati, R., Priatna, T., & Ismail, N. (2019, 25-26 July 2019). A Novel Approach to Calculating Yaw Angles Using an Accelerometer Sensor. Paper presented at the 2019 IEEE 5th International Conference on Wireless and Telematics (ICWT).
- O'connor, B. J., & Zomick, D. A. (1976). Attitude Determination Algorithm for a Strapdown IMU. *IFAC Proceedings Volumes*, 9(1), 397-411. doi:10.1016/S1474-6670(17)67138-6
- Overholser, R., & Xu, R. (2014). Effective degrees of freedom and its application to conditional AIC for linear mixed-effects models with correlated error structures. *Journal of Multivariate Analysis*, 132, 160-170. doi:<https://doi.org/10.1016/j.jmva.2014.08.004>
- Paredes, J. A., Álvarez, F. J., Aguilera, T., & Villadangos, J. M. (2017). 3D Indoor Positioning of UAVs with Spread Spectrum Ultrasound and Time-of-Flight Cameras. *Sensors (Basel, Switzerland)*, 18(1). doi:10.3390/s18010089
- Park, H., Noh, J., & Cho, S. (2016). Three-dimensional positioning system using Bluetooth low-energy beacons. *International journal of distributed sensor networks*, 12(10), 155014771667172. doi:10.1177/1550147716671720
- Passaro, V. M. N., Cuccovillo, A., Vaiani, L., Carlo, M. D., & Campanella, C. E. (2017). Gyroscope Technology and Applications: A Review in the Industrial Perspective. *Sensors (Basel)*, 17(10), 2284. doi:10.3390/s17102284
- Phillips, N. (2012). Gold exploration success. *Applied Earth Science (Transactions of the Institution of Mining and Metallurgy, Section B)*, 120(1), 7-20. doi:10.1179/1743275811Y.0000000019
- Rees, C. (2020). Selecting an Inertial Measurement Unit (IMU) for UAV Applications. Retrieved from <https://www.unmannedsystemstechnology.com/feature/selecting-an-inertial-measurement-unit-imu-for-uav-applications/>

- Reliant Systems, I. (2019). The Six Degrees Of Freedom. Retrieved from <https://www.reliantsystemsinc.com/the-six-degrees-of-freedom/>
- Report, Q. A. (2003). Queensland Centre for Advanced Technologies. Retrieved from <https://research.csiro.au/qcat/wp-content/uploads/sites/332/2019/10/QCAT-AnnualReport-03-04.pdf>
- Roberts, J. M., Duff, E. S., Corke, P. I., Sikka, P., Winstanley, G. J., & Cunningham, J. (2000). Autonomous control of underground mining vehicles using reactive navigation (Vol. 4, pp. 3790-3795).
- Robertson, H. P. (1949). Postulate versus Observation in the Special Theory of Relativity. *Reviews of Modern Physics*, 21(3), 378-382. doi:10.1103/RevModPhys.21.378
- Ron Harrison, H. (2007). *Engineering Mechanics (Vol. 2) – Dynamics – Sixth edition* J.L. Meriam and L.G. Kraige John Wiley and Sons, The Atrium, Southern Gate, Chichester, West Sussex, PO19 8SQ. 2007. 720pp. Illustrated. £89.95. ISBN 0-471-73931-6. *Aeronautical journal*, 111(1120), 406. doi:10.1017/S0001924000086978
- Rongyan, W., Minming, T., & Shoufeng, T. (2017). Application of bluetooth communication in mine environment detection vehicle (pp. 236-239): IEEE.
- Seong-hoon, W., Melek, W., & Golnaraghi, F. (2008). Position and orientation estimation using Kalman filtering and particle filtering with one IMU and one position sensor (pp. 3006-3010): IEEE.
- Shahmoradi, J., Talebi, E., Roghanchi, P., & Hassanalian, M. (2020). A Comprehensive Review of Applications of Drone Technology in the Mining Industry. *Drones (Basel)*, 4(3), 34. doi:10.3390/drones4030034
- Shawn. (2020). Accelerometer vs Gyroscope sensor, and IMU, how to pick one? Retrieved from <https://www.seeedstudio.com/blog/2019/12/24/what-is-accelerometer-gyroscope-and-how-to-pick-one/>
- Smyth, A., & Wu, M. (2007). Multi-rate Kalman filtering for the data fusion of displacement and acceleration response measurements in dynamic system monitoring. *Mechanical Systems and Signal Processing*, 21(2), 706-723. doi:10.1016/j.ymssp.2006.03.005
- Stephenson, F. R. (2003). Historical eclipses and Earth's rotation. *Astronomy & Geophysics*, 44(2), 2.22-22.27. doi:10.1046/j.1468-4004.2003.44222.x
- Tak Kit, L., Yun-Hui, L., & Kai Wun, L. (2013). Inertial-Based Localization for Unmanned Helicopters Against GNSS Outage. *IEEE Transactions on Aerospace and Electronic Systems*, 49(3), 1932-1949. doi:10.1109/TAES.2013.6558029
- TDK. (2021). MPU-9250. Retrieved from <https://invensense.tdk.com/products/motion-tracking/9-axis/mpu-9250>
- Thompson, M. K., & Thompson, J. M. (2017). Chapter 3 - Creating and Importing Geometry. In M. K. Thompson & J. M. Thompson (Eds.), *ANSYS Mechanical APDL for Finite Element Analysis* (pp. 47-65): Butterworth-Heinemann.
- Thuillier, J. (2018). Handling IMU Drift. Retrieved from <https://vrtracker.xyz/handling-imu-drift/>
- Townsend, K. (2020). Adafruit 10-DOF IMU Breakout. Retrieved from <https://learn.adafruit.com/adafruit-10-dof-imu-breakout-lsm303-l3gd20-bmp180>

- Vázquez-Arellano, M., Griepentrog, H. W., Reiser, D., & Paraforos, D. S. (2016). 3-D Imaging Systems for Agricultural Applications-A Review. *Sensors (Basel)*, 16(5), 618. doi:10.3390/s16050618
- Velodyne LiDAR, I. (2019). How does LiDAR work? Retrieved from <http://www.lidar-uk.com/how-lidar-works/>
- Wang, M., Cao, H., Shen, C., & Chai, J. (2018). A Novel Self-Calibration Method and Experiment of MEMS Gyroscope Based on Virtual Coriolis Force. *Micromachines*, 9(7), 328. doi:10.3390/mi9070328
- Wang, Y., & Rajamani, R. (2018). Direction cosine matrix estimation with an inertial measurement unit. *Mechanical Systems and Signal Processing*, 109, 268-284. doi:10.1016/j.ymsp.2018.02.038
- White, A. J. A., Joughin, N. C., & Cook, N. G. W. (1975). IMPROVEMENTS IN STOPE DRILLING AND BLASTING FOR DEEP GOLD MINES. *Journal of The South African Institute of Mining and Metallurgy*, 75(6), 139-150.
- Woodford, C. (2020). Accelerometers. Retrieved from <https://www.explainthatstuff.com/accelerometers.html>
- Xuhui, H., Wei, Z., & Dongxin, L. (2010). Underground miners localization system based on ZigBee and WebGIS (pp. 1-5): IEEE.
- You, Z. e. (2018). *Space microsystems and micro/nano satellites* / edited by Zheng You: Oxford, [England] : Butterworth-Heinemann.
- Yuping, Z., Yinghui, Z., & Chen, L. (2014). Research of Short Distance Wireless Communication Technology in the Mine Underground (pp. 955-959).
- Zhang, J., Welch, G., Bishop, G., & Huang, Z. (2014). A Two-Stage Kalman Filter Approach for Robust and Real-Time Power System State Estimation. *IEEE transactions on sustainable energy*, 5(2), 629-636. doi:10.1109/TSTE.2013.2280246